NASA TECHNICAL NOTE

NASA TN D-4337

NASA TN D-4337

C. 1

[illegible] RE
A[illegible] (WLI
KIRTLAND AFB,

0131229

TECH LIBRARY KAFB, NM

EXPERIMENTAL STABILITY AND CONTROL RESULTS AT MACH 19 OF AN ENTRY VEHICLE DESIGNED FOR AN INTERMEDIATE LIFT-DRAG RATIO

by Patrick J. Johnston and Robert D. Witcofski

Langley Research Center
Langley Station, Hampton, Va.

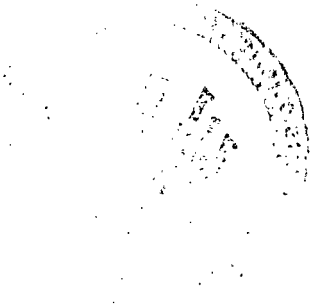

NATIONAL AERONAUTICS AND SPACE ADMINISTRATION • WASHINGTON, D. C. • FEBRUARY 1968

TECH LIBRARY KAFB, NM
0131229

EXPERIMENTAL STABILITY AND CONTROL RESULTS AT MACH 19 OF AN ENTRY VEHICLE DESIGNED FOR AN INTERMEDIATE LIFT-DRAG RATIO

By Patrick J. Johnston and Robert D. Witcofski

Langley Research Center
Langley Station, Hampton, Va.

NATIONAL AERONAUTICS AND SPACE ADMINISTRATION

For sale by the Clearinghouse for Federal Scientific and Technical Information
Springfield, Virginia 22151 – CFSTI price $3.00

EXPERIMENTAL STABILITY AND CONTROL RESULTS AT MACH 19 OF AN ENTRY VEHICLE DESIGNED FOR AN INTERMEDIATE LIFT-DRAG RATIO

By Patrick J. Johnston and Robert D. Witcofski
Langley Research Center

SUMMARY

An exploratory investigation of the longitudinal, lateral, and directional stability and control characteristics of a lifting entry vehicle has been conducted at a Mach number of 19 and a Reynolds number, based on length, of 3.05×10^6. At these conditions the boundary layer is believed to be laminar over the model. The configuration, which was characterized by a large-volume fuselage, was designed to achieve a trimmed maximum lift-drag ratio of 2.0. Realistic centers of gravity dictated by packaging studies were employed to evaluate the stability results. The effects on stability and performance of wing planform shape and size, ventral body fins, wing-tip fins, and body camber were examined. The final configuration, which included a shoulder-height wing with tip fins, achieved a trimmed maximum lift-drag ratio slightly in excess of 2.0 and was stable in pitch and sideslip over the angle-of-attack range for which it could be trimmed in pitch.

INTRODUCTION

Some recent studies at the Langley Research Center have been concerned with defining the aerodynamic principles involved in achieving high lift-drag ratios at hypersonic Mach numbers. (See, for example, refs. 1 to 4.) These studies have been of a fundamental nature and have, therefore, concentrated on optimizing simple shapes for maximum lift-drag ratios. The emphasis in more recent investigations has been on the sacrifice in performance required for trim and longitudinal, lateral, and directional stability of configurations with realistic volume distributions and center-of-gravity locations (ref. 5).

The design of manned lifting entry vehicles is often compromised by the requirement for flight over a wide range of speeds. One promising technique for circumventing the subsonic-hypersonic incompatibility problem is to decouple the landing mode from the entry mode of flight. Love (ref. 6) discusses a number of aspects of the decoupled landing technique for maneuverable entry vehicles. With the assumption that a decoupled

landing mode would be employed, the present investigation was directed toward defining a manned entry vehicle capable of a hypersonic lift-drag ratio of about 2.0 and exhibiting longitudinal, lateral, and directional stability at Mach numbers experienced shortly after entry. The effects on stability and performance of nose shape (which included cant angle, camber, and length), various wing planforms and locations, and several fins and strakes were determined for a basic body shape of sufficient volume for the convenient placement of men and equipment. The investigation was conducted in the Langley 22-inch helium tunnel at a Mach number of 19.1 and a Reynolds number of 3.05×10^6 based on the model length.

SYMBOLS

The data in the present investigation are referred to the body-axis system except for the lift and drag coefficients, which are referred to the stability-axis system.

b characteristic length for rolling moment and yawing moment (equal to width of body at base)

C_D drag coefficient, $\frac{\text{Drag}}{qS}$

C_L lift coefficient, $\frac{\text{Lift}}{qS}$

C_l rolling-moment coefficient, $\frac{\text{Rolling moment}}{qSb}$

C_m pitching-moment coefficient about moment center at $0.643l$ or $0.605l$ (see fig. 1), $\frac{\text{Pitching moment}}{qSl}$

C_N normal-force coefficient, $\frac{\text{Normal force}}{qS}$

C_n yawing-moment coefficient about moment center at $0.643l$ or $0.605l$ (see fig. 1), $\frac{\text{Yawing moment}}{qSb}$

C_Y side-force coefficient, $\frac{\text{Side force}}{qS}$

$C_{l_\beta} = \left(\Delta C_l / \Delta\beta\right)_{\beta \approx 0^\circ, 5^\circ}$, per deg

$C_{n_\beta} = \left(\Delta C_n / \Delta\beta\right)_{\beta \approx 0^\circ, 5^\circ}$, per deg

$C_{Y_\beta} = \left(\Delta C_Y/\Delta\beta\right)_{\beta \approx 0^o,5^o}$, per deg

L/D	lift-drag ratio
$(L/D)_{max}$	maximum lift-drag ratio
l	body length (see fig. 1)
q	dynamic pressure
r	radius of curvature
S	planform area of body
s	exposed wing semispan
α	angle of attack of body reference line, deg
α_{opt}	angle of attack for maximum lift-drag ratio, deg
β	angle of sideslip, deg
δ_e	elevon deflection angle, positive when trailing edge is down, deg
δ_r	deflection angle of right-hand rudder, referred to fuselage axis, deg
ϕ	fin dihedral angle defined in figure 1(l)

Model component designations:

N	nose
B	body
W	wing
F	fin
S	strake

CONFIGURATIONS

Sketches of the models employed in the investigation are shown in figure 1, and photographs of typical configurations are presented in figure 2. Geometric details of the initial fuselage shape, N_1B_1, are illustrated in figure 1(a). The moment reference center indicated in this figure corresponds to a center-of-gravity location 27 feet (8.2 m) from the nose of a 42-foot (12.8-m) vehicle and is the aft limit considered in this study. Various internal-systems layouts indicated the possibility that a realistic forward limit on the center of gravity of 25 feet (7.6 m) could be achieved. Thus, for the purpose of evaluating the stability of configurations incorporating fuselage N_1B_1, the fore and aft center-of-gravity limits were $0.594l$ and $0.643l$, respectively.

During the course of the investigation, the effects on stability and performance of several variations in nose shape were determined; these included variations in cant angle, camber, and length. The original nose shape and the modifications are shown in figures 1(b) to 1(e). The shorter models in these figures correspond to a full-scale length of 38 feet (11.6 m); and since they represented only a small change in the longitudinal volume distribution, it was assumed that the full-scale center of gravity would remain a fixed distance from the fuselage base. Thus, for the configurations shown in figures 1(c) and 1(e), the corresponding full-scale center-of-gravity limits range from 21 to 23 feet (6.4 to 7.0 m, or $0.553l$ to $0.605l$).

During the initial phase of the investigation, three wing planforms were studied; these are shown in figures 1(f) to 1(h). The vertical locations of the wings were such that the root chord of the upper surface coincided with the fuselage reference line. The lower surface of these wings was flat, and provisions were made for trailing-edge elevons as illustrated. Wings W_1 to W_3 were somewhat unusual in upper surface contour; the root-chord thickness was constant (and corresponded to 6 inches, or 15.2 cm, for the full-scale vehicle), and at the point where the wing leading edge joined the body, the upper surface blended into the vertical side of the fuselage. Moving rearward of this intersection, the lines generating the upper surface rotate toward the horizontal reference plane of the body. The concept of a constant root-chord thickness was employed in an attempt to simplify the wing attachment and alleviate potential thermostructural problems.

As the investigation proceeded and it became apparent that more stabilizing area would be required, additional wings were fabricated; these wings, designated W_4 and W_5, are shown in figures 1(i) and 1(j). Unlike the previous group of three wings, these had constant upper-surface wedge angles; their vertical location on the fuselage was the same as that of the first three wings, however.

Various fuselage fins and strakes were also investigated and are shown in figures 1(l), 1(m), and 1(n). The fins were fabricated of 0.040-inch-thick (1.016-mm) brass

sheet and incorporated a 15^{o} bevel on the leading edges. This bevel was situated so that it was on the leeward side of the fin when the configuration was at positive angles of attack. The strake shown in figure 1(m) was 0.008 inch (0.2032 mm) thick and was located in the reference plane of the body. Although the thickness ratios of the various fins and strakes were not realistic, their dimensions facilitated fabrication and permitted a quick assessment of their stabilizing effectiveness. Duplication of realistic thickness ratios for the purpose of accurate performance measurements was of secondary importance in this phase of the investigation.

Two configurations were studied in the final phases of the investigation; they are shown in figures 1(o) and 1(p). Both incorporate wing W_4 modified to allow for tip fins with a 10^{o} toe-in angle. The configuration shown in figure 1(p) had rudder panels mounted on the sides of the fuselage and wing trailing-edge controls. The fin leading edges were beveled on the inboard surfaces.

One modification was made to body B_1 during the investigation. This body, designated B_2, is shown in figure 1(f). The modification consisted of filling in the area adjacent to the body and beneath wing W_1. This fairing was blended into the lower contour of the fuselage.

For the purpose of comparing various configurations and evaluating the contributions of various components, the body planform area, length, and width at the base were employed to reduce the force and moment data to coefficient form. The reference values are given in table I and the actual model values are given in table II.

TABLE I.- REFERENCE AREAS AND LENGTHS

Configuration	S		l		b	
	in^2	cm^2	in.	cm	in.	cm
N_1B_1	22.001	141.94	15.000	38.100	2.286	5.806
N_2B_1	21.559	139.09	13.572	34.473	2.286	5.806
N_3B_1	22.001	141.94	15.000	38.100	2.286	5.806
N_4B_1	21.006	135.52	13.572	34.473	2.286	5.806
N_1B_2	22.001	141.94	15.000	38.100	2.286	5.806

TABLE II.- ACTUAL MODEL AREAS AND LENGTHS

Configuration	S		l		b	
	in^2	cm^2	in.	cm	in.	cm
N_1B_1	22.001	141.94	15.000	38.100	2.286	5.806
N_2B_1	21.559	139.09	13.572	34.473	2.286	5.806
N_3B_1	22.001	141.94	15.000	38.100	2.286	5.806
N_4B_1	21.006	135.52	13.572	34.473	2.286	5.806
N_1B_2	26.784	172.80	15.000	38.100	3.572	9.073
$N_1B_1W_1$	26.784	172.80	15.000	38.100	3.572	9.073
$N_1B_1W_2$	30.355	195.84	15.000	38.100	3.572	9.073
$N_1B_1W_3$	32.651	210.65	15.000	38.100	3.572	9.073
$N_1B_1W_4$	32.176	207.59	15.000	38.100	5.000	12.700
$N_1B_1W_5$	35.926	231.78	15.000	38.100	6.000	15.240
$N_4B_1W_1$	25.829	166.64	13.572	34.473	3.572	9.073
$N_4B_1W_4$	31.184	201.19	13.572	34.473	5.000	12.700
$N_2B_1W_1$	26.382	170.21	13.572	34.473	3.572	9.073

APPARATUS AND TESTS

The investigation was conducted at a nominal free-stream Mach number of 19.1 in the Langley 22-inch helium tunnel. Operational characteristics of this facility are given in reference 7 and details of the flow characteristics of the contoured nozzle (in which the present tests were made) are available in reference 8. Stagnation pressures were automatically regulated at 500 psig (3447 kN/m^2). Stagnation temperatures diminished during the course of each test as a result of the decreasing reservoir pressure; measurements indicate an average of about 80° F (300° K). At a stream Mach number of 19.1, these stagnation conditions provided a Reynolds number, based on a model length of 15.00 inches (38 cm), of 3.05×10^6. On the basis of the experimental work reported in reference 9, it is presumed that the boundary layer over the model was laminar for the present investigation.

The models, which were attached to internal, sting-mounted strain-gage balances, were continuously pitched during the course of each test. The balance and base-pressure-transducer outputs were sampled and recorded on a high-speed analog-to-digital recording system twice at the selected angles of attack: once when the model was being pitched in the positive direction and again when the model was pitched in the negative direction. Generally, only the average of these two sets of data (at the same α) are presented; however, when differences are large enough to be apparent on the plots, both sets of data are shown to indicate their magnitudes. Details of the data-acquisition techniques employed in this tunnel are available in reference 7.

Base pressures were measured for the purpose of adjusting the balance axial forces to a condition where free-stream pressure acted over the fuselage base area. For these measurements, a small, high-response differential pressure transducer was located outside the tunnel wall with the sensing side of the transducer attached to tubing of 0.090-inch (2.3-mm) inside diameter which, in turn, was taped to the model support sting. Pressures on the reference side of the transducer were maintained at approximately 10 microns of mercury. The transducer was calibrated before each test. Experience with this technique of simultaneous force and pressure measurements on a continuously pitching model has shown that, although the pressure transducer experiences a small time lag due to the length of tubing from the model base to the gage, the errors in pressure are of such a small magnitude that the resulting increments in axial force are generally within the accuracy range of the strain-gage balance.

RESULTS AND DISCUSSION

Exploratory Results

Longitudinal stability and performance data obtained on configuration N_1B_1 in combination with wings W_1, W_2, and W_3 are shown in figures 3, 4, and 5, respectively. The performance data indicate that these configurations achieved maximum lift-drag ratios somewhat above 2. The stability data indicate that with wings W_1, W_2, and W_3, the configuration is unstable about a center of gravity at $0.643l$. For trim to occur at $\alpha_{opt} \approx 8^o$ with zero elevon deflection, wing W_1 would require a center-of-gravity location at 51.7 percent of the body length. Similarly, wings W_2 and W_3 would require centers of gravity at 52.6 and 50.4 percent of the length. It is noted that these centers of gravity are all well ahead of the forward limit of $0.594l$ which packaging studies had previously indicated to be realistic.

An inspection of the results in figures 3 to 5 shows that the elevon effectiveness varied considerably over the angle-of-attack range. Negative elevon deflections, for example, were much more effective at negative angles of attack than corresponding deflections at positive angles of attack. This greater effectiveness is believed to be

associated with extensive regions of separated flow over the upper surfaces of the configuration which are promoted by the negatively deflected controls. It is also of interest to note that the control effectiveness near an angle of attack of zero was somewhat greater for wing W_1 than for wings W_2 and W_3. This behavior is apparently due to the longer root chord of the latter wings, which would cause thicker boundary layers at the elevons. At angles of attack near $(L/D)_{max}$, the control effectiveness for all three wings was essentially the same, indicating a more nearly equivalent flow condition on the three wings.

Figure 6 contains the stability and performance results obtained on configuration $N_2B_1W_1$, which incorporates a shorter and more highly cambered nose than N_1. As a result of the slightly blunter nose, some loss in maximum lift-drag ratio occurred for this configuration as compared with $N_1B_1W_1$ (from about 2.25 to 2.0). It was determined from figure 6(b) that configuration $N_2B_1W_1$ could be trimmed at $(L/D)_{max}$ with a center of gravity at $0.462l$ which, again, is well ahead of the forward limit of $0.553l$ specified by systems studies and internal-equipment layouts.

Inasmuch as the configurations incorporating noses N_1 and N_2 and wings W_1, W_2, and W_3 were unstable about the center-of-gravity locations selected on the basis of packaging requirements, several modifications to improve the stability were investigated. These alterations included wings W_4 and W_5 and body B_2. The wings, which have the same root-chord length as wing W_1, represent planform-area additions, while N_1B_2, which has the same planform area as $N_1B_1W_1$, represents an appreciable increase in fuselage volume. The effects of these modifications are summarized in figure 7. Also included for comparison are the data obtained on the isolated body, N_1B_1, and the wing-body combination, $N_1B_1W_1$.

As expected, the performance data in figure 7(a) indicate that the additional wing area improves the maximum lift-drag ratio while configuration N_1B_2, which represents additional volume, has a lower maximum lift-drag ratio than the isolated body N_1B_1. Figure 7(a) also includes some interesting information concerning the lift effectiveness of the various wings and bodies. For example, at positive angles of attack wing W_1 did not provide significant increases in lift coefficient over that obtained for the isolated body, N_1B_1. Further, the high-volume configuration, N_1B_2, which has a projected planform area equivalent to $N_1B_1W_1$, achieved nearly the lift of $N_1B_1W_4$ despite the fact that the increase in width (in excess of the isolated body) was only 47 percent of that for wing W_4. Thus, it may be inferred from the small increments in lift provided by the slenderest wing, W_1, and the sizable increments provided by body N_1B_2 that, for the particular body shape of this investigation, the lifting surfaces are relatively ineffective as a result of their placement at the shoulder.

The stability results of the five configurations are compared in figure 7(b), where the pitching moments are referred to the rearward center-of-gravity limit, $0.643l$.

The configuration incorporating wing W_5 was the only one of those shown that could be trimmed at α_{opt} within the center-of-gravity limits specified (0.643l to 0.594l) and also the only one that possessed positive longitudinal stability when trimmed at the angle of attack for $(L/D)_{max}$.

The small increments in lift between the isolated body and, for example, configuration $N_1B_1W_1$ prompted a closer examination of the effect of increasing the span of the wing on normal force and pitching moment. The experimental increments in C_N and C_m due to the addition of the various wings to the body are compared in figure 8 with calculations based on flat-plate-modified impact theory (ref. 10) assuming isolated panels. The wing contributions to C_N and C_m are shown in figure 8(a) as a function of the angle of attack. These data have been cross-plotted in figure 8(b) to indicate the wing contributions at a fixed angle of attack near $(L/D)_{max}$. It is apparent from these results that the wings do not act as isolated panels and that the flow fields about these configurations are dominated by the relatively large fuselage. Further, it is anticipated that these interference effects will vary considerably over the flight Mach number range in which the vehicle operates in the entry flight mode.

Nose Camber and Cant

One technique for limiting the forward center-of-gravity shift necessary to trim these vehicles at $(L/D)_{max}$ is to reduce the pitching moment by decreasing the camber or cant angle of the nose. Two modified versions of noses N_1 and N_2 were fabricated. Nose N_3 had the same length and planform area as N_1. Nose N_4 had the same length as nose N_2 but had a somewhat smaller projected planform area inasmuch as in the planform view it was composed of straight-line elements (compare figs. 1(c) and 1(e)).

Figures 9 and 10 summarize the results obtained by varying the cant angle and camber on the long- and short-nosed configurations. It is observed that reducing the cant angle and camber resulted in beneficial increments in pitching moment along with moderate improvements in maximum lift-drag ratio.

Ventral Fins

Inasmuch as the isolated body achieved a maximum lift-drag ratio of 2.2, which was greater than the original goal of 2.0, and since it was desirable to minimize the lifting surfaces added to this body, other devices were considered for the purpose of obtaining longitudinal stability. In view of the previous results with the shoulder-height wings, one expedient which suggested itself was stabilizing surfaces mounted on the lower rear portion of the body. The fins chosen for this phase of the investigation are shown in figure 1(l). They were tested at both positive and negative dihedral angles as well as at zero dihedral. The longitudinal characteristics of the N_4B_1 configuration with the

various fins are shown in figures 11(a) and 11(b); the moment data are referred to a fuselage station at $0.605l$.

The performance data in figure 11(a) indicate that the addition of the fins did not significantly affect the maximum lift-drag ratio. It is of interest to note that at zero angle of attack the fins produced negative lift increments, while at angles of attack greater than 2°, positive increments were realized. Beyond $\alpha = 2^{\circ}$ the upward canted fin, F_8, provided the smallest increment in lift.

The longitudinal stability results obtained with these fins (fig. 11(b)) show that at zero angle of attack all but fin F_7 (canted down 45°) provided a positive increment in pitching moment. These positive increments in C_m at low angles of attack are probably associated with the location of the fins in the flow field of the nose. Ordinarily, in the absence of these local flow-field effects, the axial-force contribution of the fins would be expected to yield a negative increment in pitching moment. In the present instance, however, the flow direction in the neighborhood of the fins apparently is such that the flow impinges on the upper surface of the fin, yielding a negative increment in normal force and a net positive increment in pitching moment at low angles of attack. It is observed in figure 11(b) that the downward canted fins, F_6 (at -30°) and F_7 (at -45°), yield somewhat smaller increments than the uncanted fin, F_5. As the angle of attack increases, the fins move out of the nose flow field and begin providing negative inputs to pitching moment. Fin F_8, which was canted upward 30°, provided a somewhat smaller stabilizing input than the other fins at the higher angles of attack.

From the results in figure 11(b), it was determined that configuration N_4B_1 could be trimmed with positive stability at $(L/D)_{max}$ with fins F_5, F_6, and F_7 with a center of gravity located at $0.571l$, which was within the specified forward limit of $0.553l$. The selection of a center of gravity at $0.571l$, however, results in an unstable configuration below $\alpha = 4^{\circ}$ and thus limits the potential trim capabilities of the vehicle.

The lateral and directional characteristics of configuration N_4B_1 are shown in figure 11(c). It is noted that, although the fins were effective stabilizing surfaces in pitch, the isolated body did not possess sufficient lateral stability to overcome the negative dihedral effect introduced by the fins, particularly at low angles of attack. Further, the fins that were most effective in pitch (F_5 and F_6) provided the largest destabilizing roll inputs. The variation with angle of attack of the fin contribution to rolling moment is associated with the impingement of the flow from the nose on the upper surface of the windward fin, and the adverse roll contribution is observed to diminish at the higher angles of attack as the fins move out of the flow field created by the nose.

The isolated body is directionally unstable about a moment center at $0.605l$, according to the results in figure 11(c). As expected, the downward canted fin, F_6,

provided the largest stabilizing input to yawing moment as a result of its greatest projected side area. This input is observed to diminish as the angle of attack increases, however.

In an effort to improve the lateral and directional characteristics of configuration $N_4B_1F_5$, it was tested with the addition of a strake (fig. 1(m)) and an upward canted fin (F_9, fig. 1(m)), and the results are given in figure 12.

The performance data in figure 12(a) indicate no changes in lift at positive angles of attack, but a higher drag and a subsequent loss in L/D as a result of adding either the strake or fin F_9. Both the strake and fin F_9 increased the stability of the configuration; the increments were small however (fig. 12(b)).

Lateral and directional characteristics of the $N_4B_1F_5$ configuration incorporating the strake S_1 and the fuselage fin F9 are shown in figure 12(c), where it may be observed that either surface provided stabilizing inputs in C_{l_β} and C_{n_β}. With fin F_9, for example, the configuration becomes laterally stable at $\alpha = 4^o$ but still requires substantial increases in yawing moment to realize directional stability, even when the moment data are transferred to a center of gravity at $0.583l$, which, according to the data in figure 12(b), would allow the vehicle to be trimmed in pitch at the angle of attack for $(L/D)_{max}$. Although the addition of a body dorsal fin could have provided the necessary increment in yawing moment, as well as beneficial rolling-moment inputs at low angles of attack, the shielding effect of the body on such a fin at high angles of attack would have resulted in a serious deterioration in directional stability. Thus, on the basis of these and other considerations, the more attractive approach for realizing longitudinal, lateral, and directional stability was to employ a pair of tip fins mounted on one of the wings previously investigated. Stability results for configuration $N_4B_1W_4$ are presented in the following section. However, unlike the previous results on this wing which were obtained with the long fuselage N_1B_1, the moment data will be referred to the rearward center-of-gravity limit for the N_1B_1 fuselage, which is at $0.605l$.

Performance and Stability of Configuration $N_4B_1W_4$

For this phase of the investigation the tips of wing W_4 were modified to provide a toe-in angle of 10^o for the fins, F_{10}. Performance data on the isolated body, N_4B_1, the wing-body combination, $N_4B_1W_4$, and the complete configuration, $N_4B_1W_4F_{10}$, are shown in figure 13(a). Although the tip fins caused no reduction in lift, their appreciably higher drag reduced the maximum lift-drag ratio somewhat, so that the resulting $(L/D)_{max}$ for the complete configuration approximately equals that of the isolated body.

Figure 13(b) compares the longitudinal stability of the three configurations for a center of gravity at $0.605l$. One apparent beneficial effect of the tip fins is to increase the stability level at small normal-force coefficients. On the basis of the results

presented in figure 13(b), the $N_4B_1W_4F_{10}$ configuration can be trimmed with zero control deflection at $\alpha = 12^o$ $\left(\text{approximately } (L/D)_{max}\right)$ with a center-of-gravity position of $0.575l$, which is within the forward limit of $0.553l$. When trimmed at $(L/D)_{max}$, however, the complete configuration is slightly unstable at normal-force coefficients from 0 to about 0.08.

The stability of the three configurations in sideslip is shown in figure 13(c). It is noted that the addition of the wing to the isolated body substantially increased the angle-of-attack effect on lateral stability. The addition of the vertical tails produced a nearly constant increment in C_{l_β} for the angle-of-attack range investigated. Directionally, the vertical tails provided a sufficient increase in yawing moment to stabilize the configuration over the angle-of-attack range for a center of gravity at $0.605l$. A center-of-gravity movement to $0.575l$ (necessary for trim at $(L/D)_{max}$) will, of course, yield additional positive increments in the stability parameter C_{n_β}. It is also noted that the addition of the wing provided a small stabilizing input to yawing moment.

Although the data in figure 13 indicated that configuration $N_4B_1W_4F_{10}$ satisfied the performance requirements, could be trimmed at $(L/D)_{max}$ within the specified center-of-gravity limits, and was laterally and directionally stable, further attempts were made to improve the hypersonic characteristics. These included decreasing the vertical height of the tip fin to reduce the fin input to C_{l_β} and increasing the tail volume coefficient to increase the directional stability. The resulting configuration, designated $N_4B_1W_4F_{11}$, is shown in figure 1(p). Provisions were made for wing trailing-edge elevons, and rudders for directional control were located on the fuselage; such a location, in addition to avoiding structural complications associated with fin trailing-edge controls, also minimizes the adverse roll due to yaw control.

Performance results obtained on configuration $N_4B_1W_4F_{11}$ are shown in figure 14(a). Static longitudinal stability results are given in figure 14(b) for a center of gravity at $0.605l$. Trimmed characteristics for a center of gravity at $0.605l$ are summarized in figure 15(a). The maximum trimmed lift-drag ratio was about 2.2, and a -20^o elevon deflection provided a trimmed lift coefficient of 0.24 at $\alpha = 15^o$ (fig. 15(a)). Shifting the center of gravity rearward to $0.621l$ (fig. 15(b)) substantially increased the trim angle-of-attack range and available lift coefficient for an equivalent elevon deflection.

Sideslip data are shown in figure 16. It is observed that, although the magnitude of C_{l_β} was less at $\alpha = 0^o$ than for the $N_4B_1W_4F_{10}$ configuration because of decreased fin height, the additional wing area represented by the trailing-edge elevons substantially increased the effect of angle of attack on roll. Because the rudders were located on the sides of the fuselage, their inputs to roll were negligible. The yawing-moment results

in figure 16 indicate that the configuration was directionally stable over the angle-of-attack range for which it could be trimmed in pitch.

CONCLUSIONS

An exploratory investigation of the longitudinal, lateral, and directional stability and control characteristics of a lifting entry vehicle has been conducted at a Mach number of 19.1 and a Reynolds number, based on model length, of 3.05×10^6. The purpose of these studies was to define an entry-vehicle configuration capable of a hypersonic lift-drag ratio in the neighborhood of 2.0 and exhibiting longitudinal, lateral, and directional stability. The effects on stability and performance of nose shape (which included cant angle, camber, and length), various wing planforms and locations and several fins and strakes were determined for a basic body shape of sufficient volume for the convenient placement of men and equipment. The results of these studies indicate the following conclusions:

1. The isolated body, although longitudinally and directionally unstable, was capable of a maximum lift-drag ratio of 2.0.

2. Highly swept shoulder-height wings proved relatively ineffective as longitudinal stabilizing devices, inasmuch as portions of the wing area were embedded in the body flow field.

3. Ventral fins were more effective than the shoulder-height wings as pitch-stabilizing devices but did not provide adequate directional stability and, in addition, caused the body to become laterally unstable.

4. Favorable pitching-moment increments were achieved by reducing the fuselage nose cant or camber, and slight increases in maximum lift-drag ratio also resulted.

5. The final configuration, which incorporated shoulder-height wings and tip fins with a 10° toe-in angle, was stable about all three axes and could be trimmed at a maximum lift-drag ratio of 2.2 with a longitudinal center-of-gravity location at 62.1 percent of the fuselage length.

Langley Research Center,
National Aeronautics and Space Administration,
Langley Station, Hampton, Va., July 19, 1967,
124-07-02-18-23.

REFERENCES

1. Becker, John V.: Studies of High Lift/Drag Ratio Hypersonic Configurations. Proceedings of the 4th Congress of the International Council of the Aeronautical Sciences, Robert R. Dexter, ed., Spartan Books, Inc., 1965, pp. 877-910.

2. Johnston, Patrick J.; Snyder, Curtis D.; and Witcofski, Robert D.: Maximum Lift-Drag Ratios of Delta-Wing—Half-Cone Combinations at a Mach Number of 20 in Helium. NASA TN D-2762, 1965.

3. Fetterman, David E.; Henderson, Arthur, Jr.; Bertram, Mitchel H.; and Johnston, Patrick J.: Studies Relating to the Attainment of High-Lift-Drag Ratios at Hypersonic Speeds. NASA TN D-2956, 1965.

4. Fetterman, David E.: Favorable Interference Effects on Maximum Lift-Drag Ratios of Half-Cone Delta-Wing Configurations at Mach 6.86. NASA TN D-2942, 1965.

5. Woods, W. C.; Johnston, P. J.; Molloy, J. K.; and Henderson, A., Jr.: Recent Studies of Factors Affecting High Lift-Drag Ratios at M = 19 in Helium. AIAA Paper No. 67-138, Jan. 1967.

6. Love, Eugene S.: Manned Lifting Entry. Astronaut. Aeron., vol. 4, no. 5, May 1966, pp. 54-64.

7. Johnston, Patrick J.; and Snyder, Curtis D.: Static Longitudinal Stability and Performance of Several Ballistic Spacecraft Configurations in Helium at a Mach Number of 24.5. NASA TN D-1379, 1962.

8. Arrington, James P.; Joiner, Roy C., Jr.; and Henderson, Arthur, Jr.: Longitudinal Characteristics of Several Configurations at Hypersonic Mach Numbers in Conical and Contoured Nozzles. NASA TN D-2489, 1964.

9. Maddalon, Dal V.; and Henderson, Arthur, Jr.: Boundary Layer Transition at Hypersonic Mach Numbers. AIAA Paper No. 67-130, Jan. 1967.

10. Love, Eugene S.; Henderson, Arthur, Jr.; and Bertram, Mitchel H.: Some Aspects of Air-Helium Simulation and Hypersonic Approximations. NASA TN D-49, 1959.

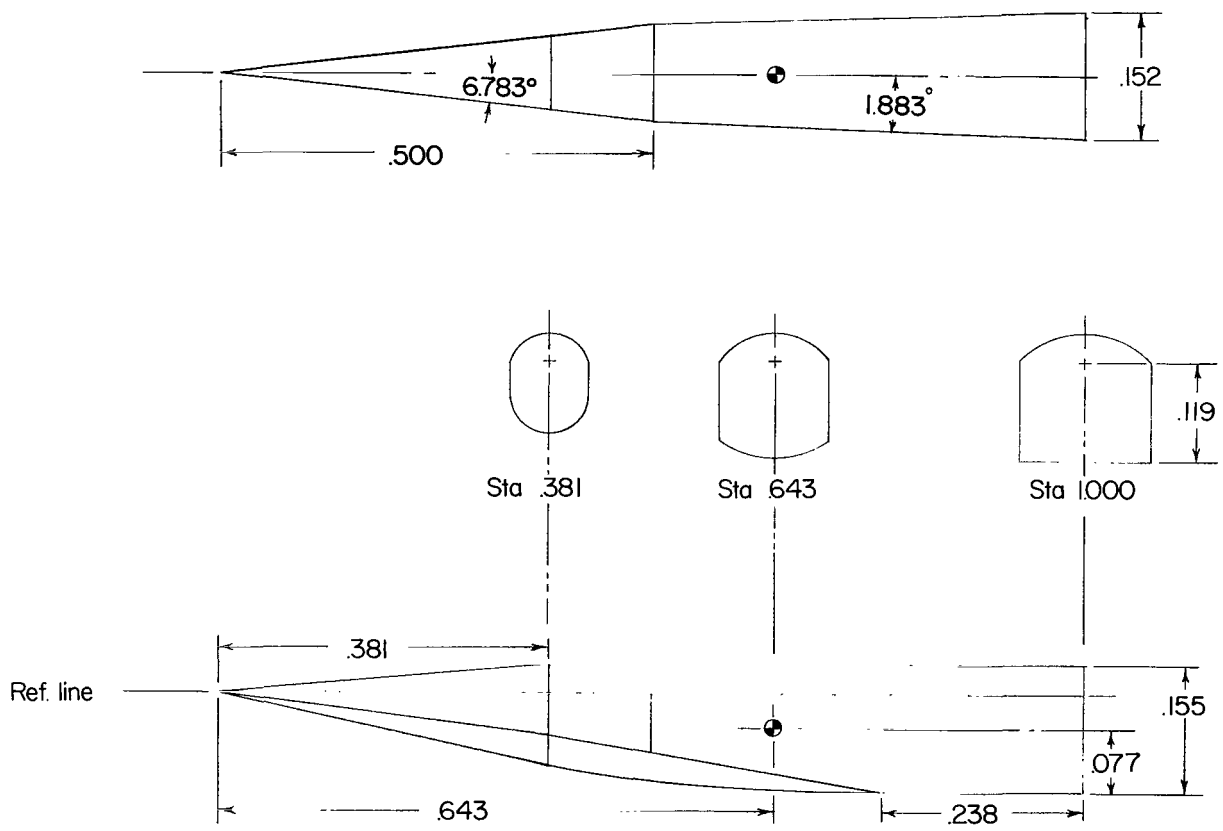

(a) Configuration N_1B_1. l = 15.000 in. (38.10 cm).

Figure 1.- Model drawings. All linear dimensions are in terms of fuselage length.

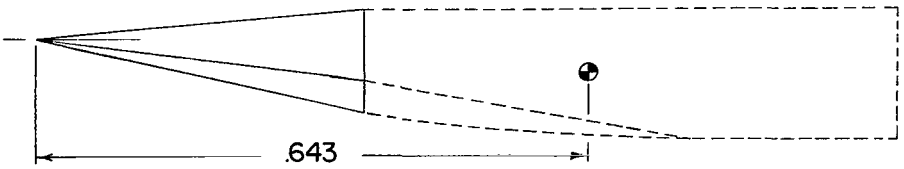

(b) Configuration N_1B_1. l = 15.00 in. (38.10 cm).

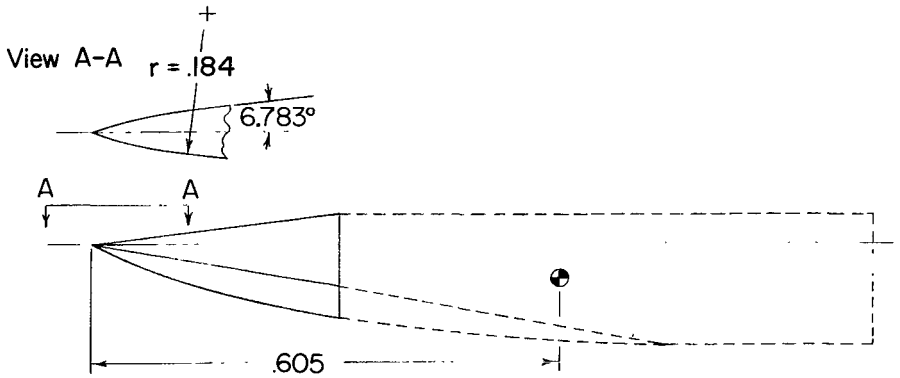

(c) Configuration N_2B_1. l = 13.572 in. (34.47 cm).

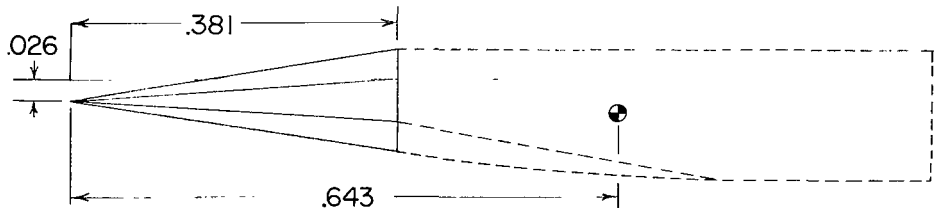

(d) Configuration N_3B_1. l = 15.000 in. (38.10 cm).

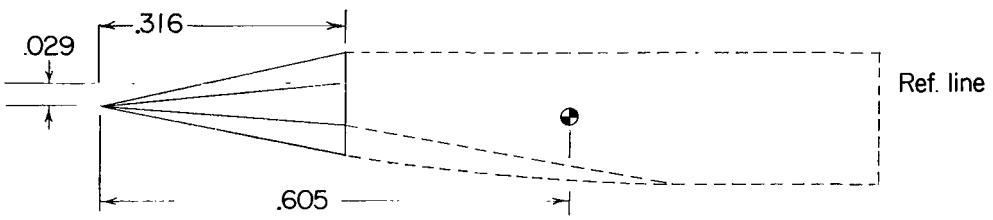

(e) Configuration N_4B_1. l = 13.572 in. (34.47 cm).

Figure 1.- Continued.

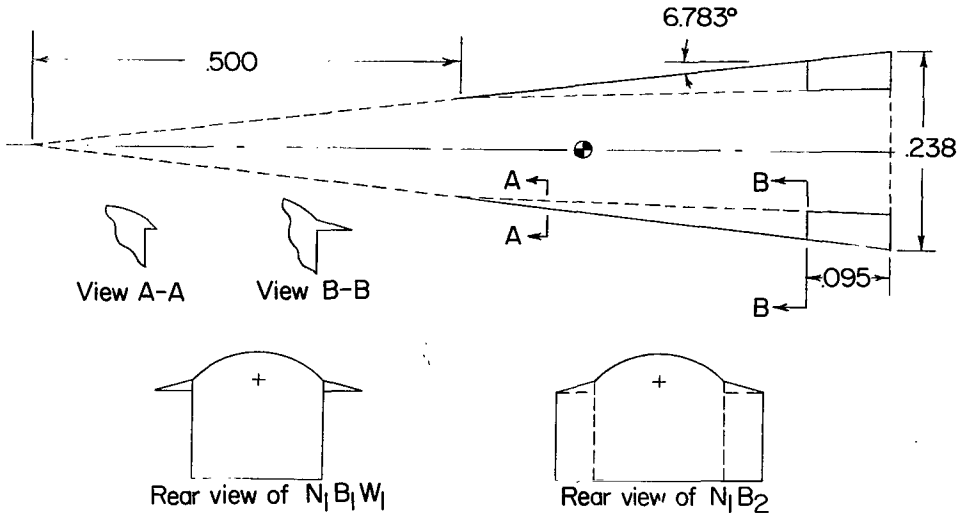

(f) Configurations $N_1B_1W_1$ and N_1B_2. l = 15.000 in. (38.10 cm).

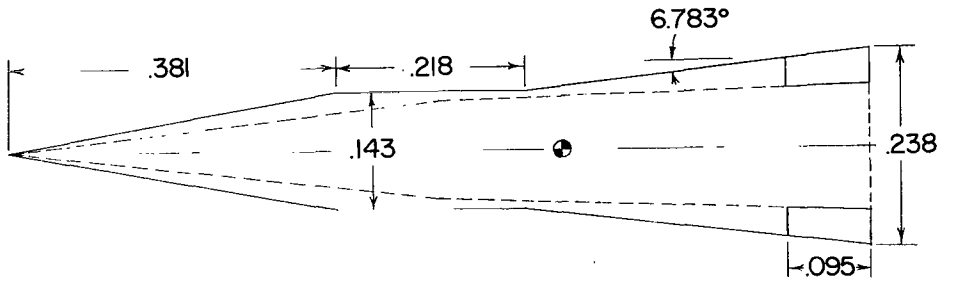

(g) Configuration $N_1B_1W_2$. l = 15.000 in. (38.10 cm).

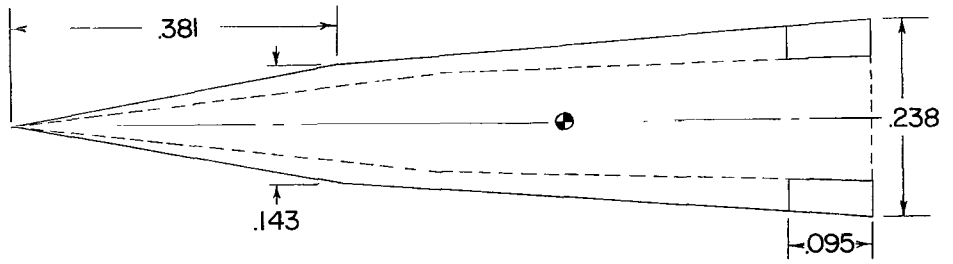

(h) Configuration $N_1B_1W_3$. l = 15.000 in. (38.10 cm).

Figure 1.- Continued.

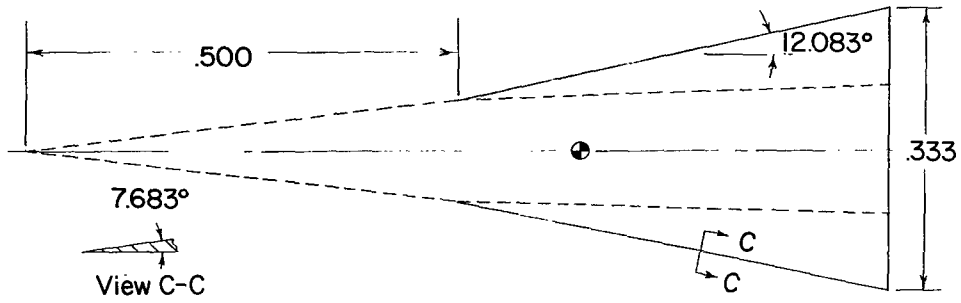

(i) Configuration $N_1B_1W_4$. l = 15.000 in. (38.10 cm).

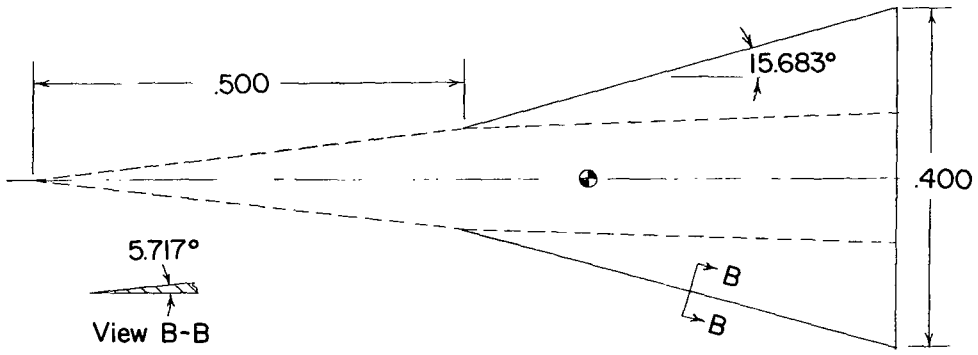

(j) Configuration $N_1B_1W_5$. l = 15.000 in. (38.10 cm).

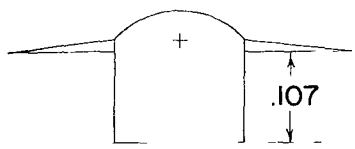

View A-A

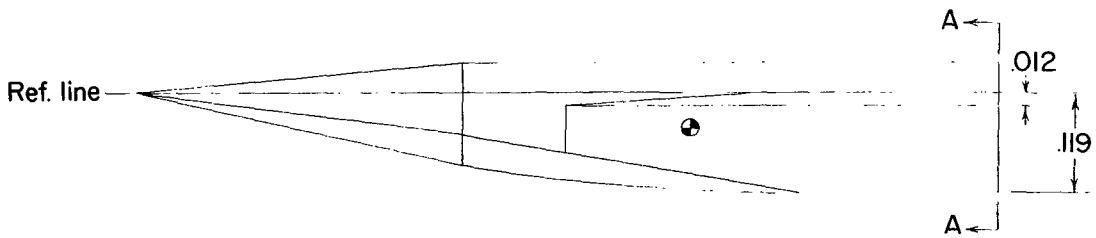

(k) Views showing typical wing installation.

Figure 1.- Continued.

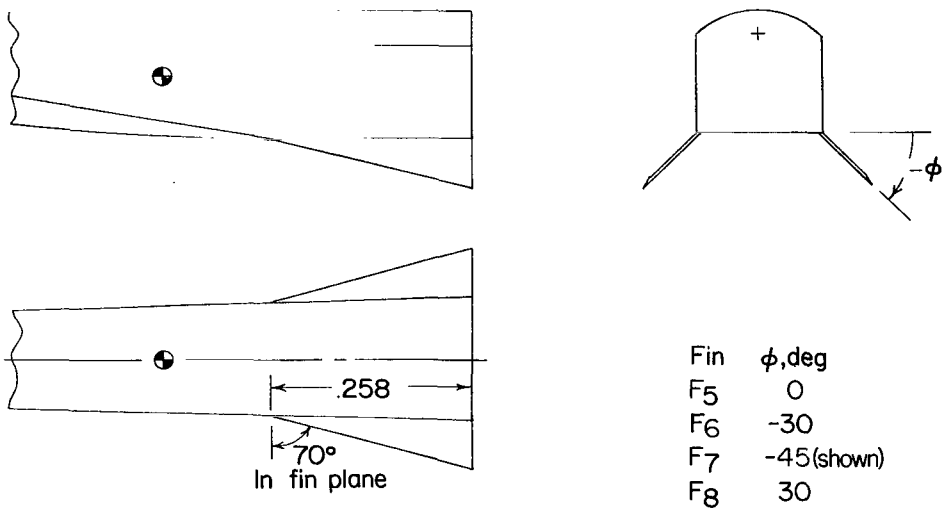

(l) Various ventral fins for configuration N_4B_1. l = 13.572 in. (34.47 cm).

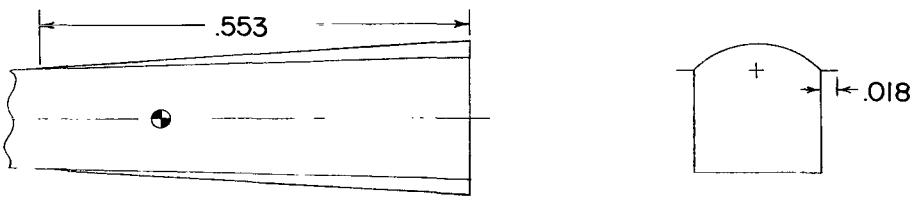

(m) Strake S_1 for configuration N_4B_1.

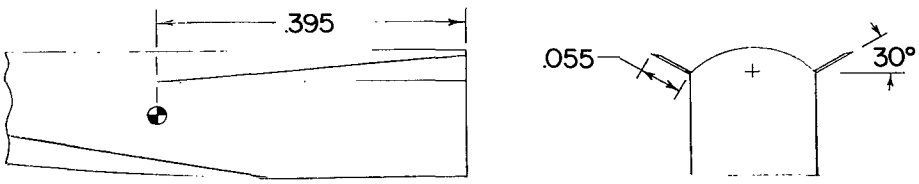

(n) Upper body fin F_9 for configuration N_4B_1.

Figure 1.- Continued.

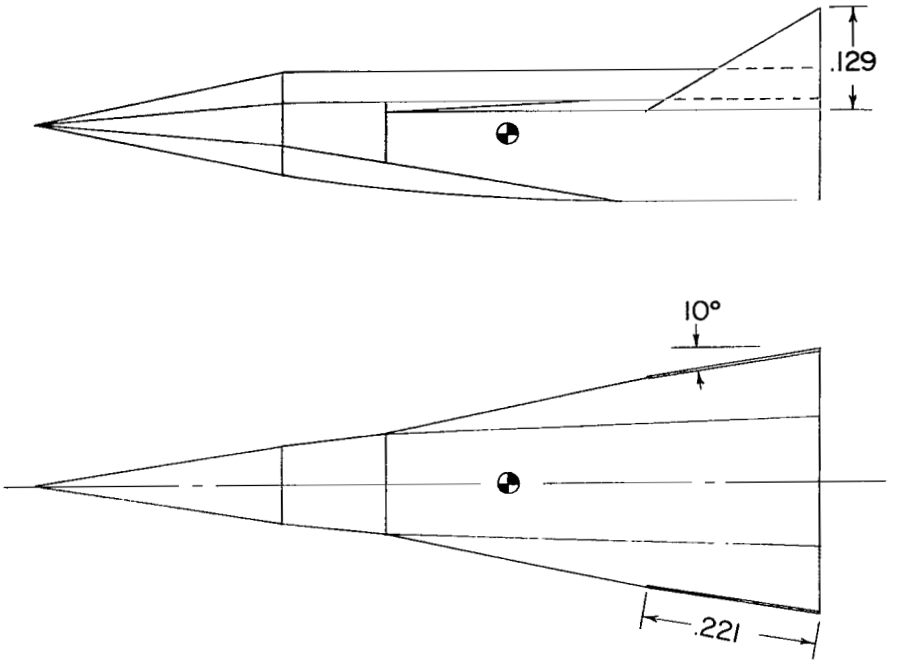

(o) Configuration $N_4B_1W_4F_{10}$. l = 13.572 in. (34.47 cm).

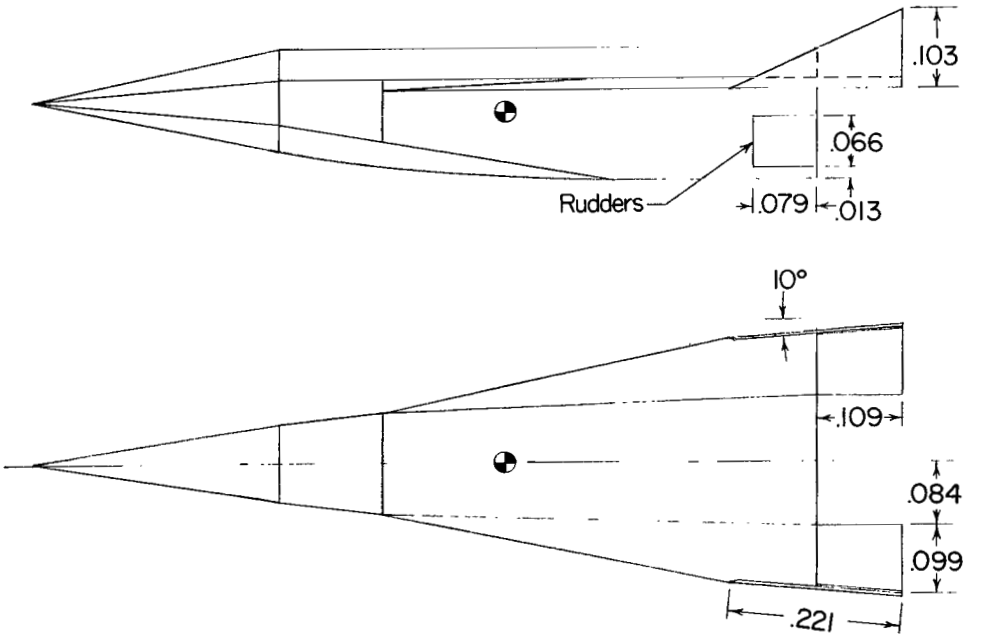

(p) Configuration $N_4B_1W_4F_{11}$.

Figure 1.- Concluded.

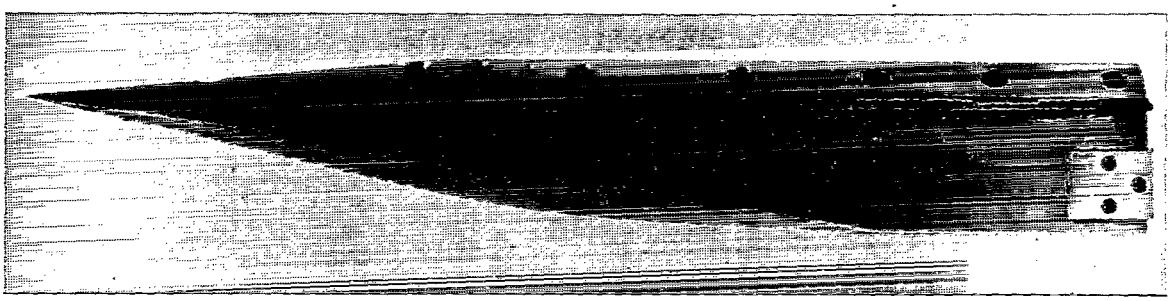

(a) Side view of configuration $N_1B_1W_1$. L-65-7438

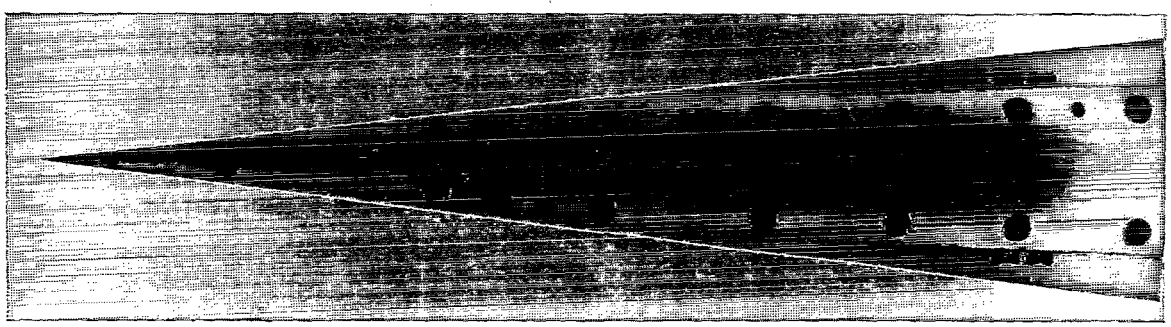

(b) Top view of configuration $N_1B_1W_1$. L-65-7439

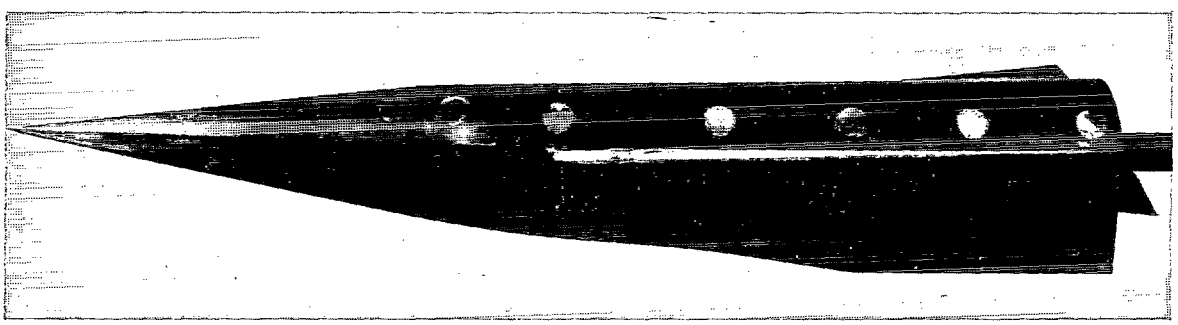

(c) Side view of configuration $N_1B_1W_5$. L-65-8300

Figure 2.- Model photographs.

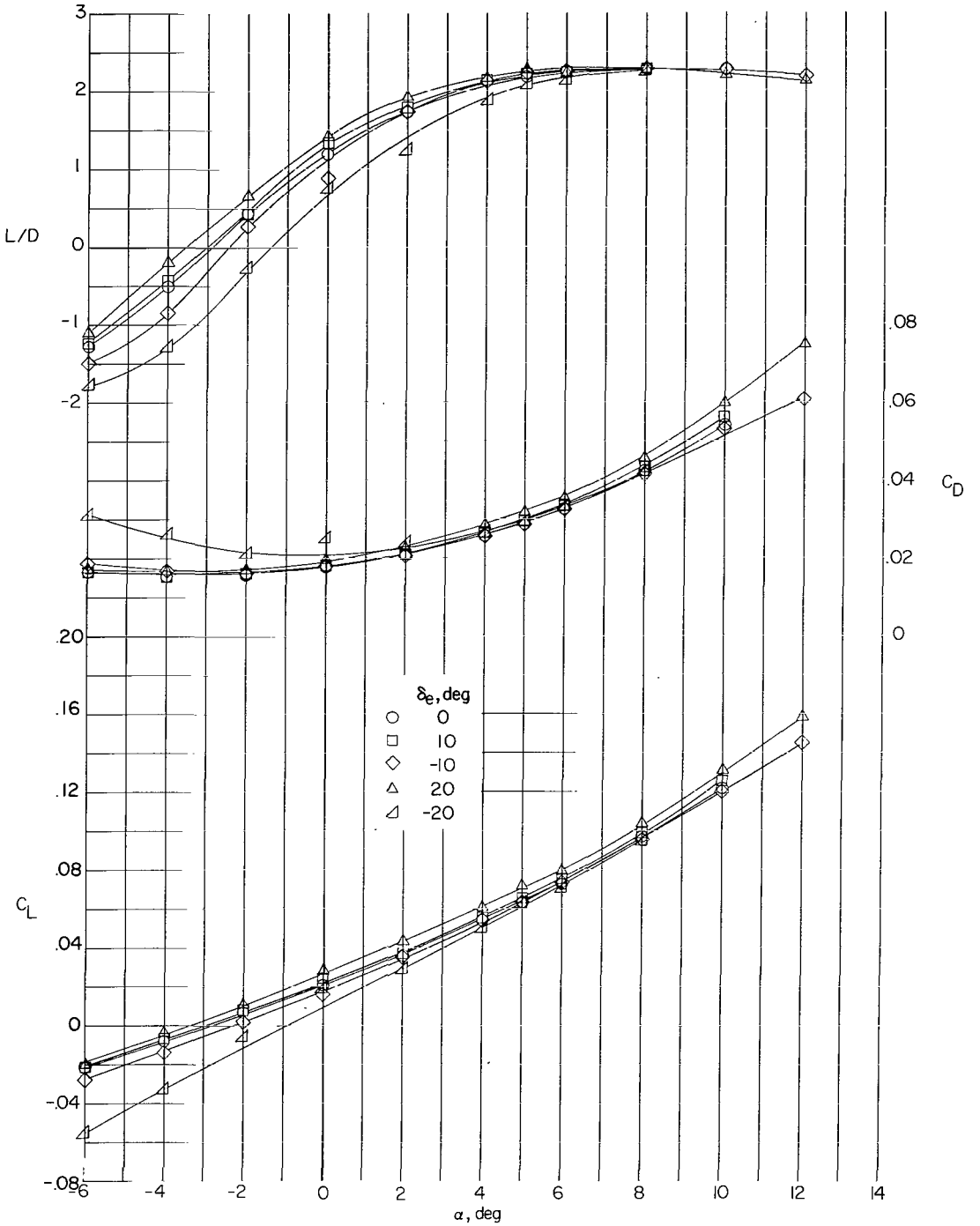

(a) Performance.

Figure 3.- Stability and performance of configuration $N_1B_1W_1$.

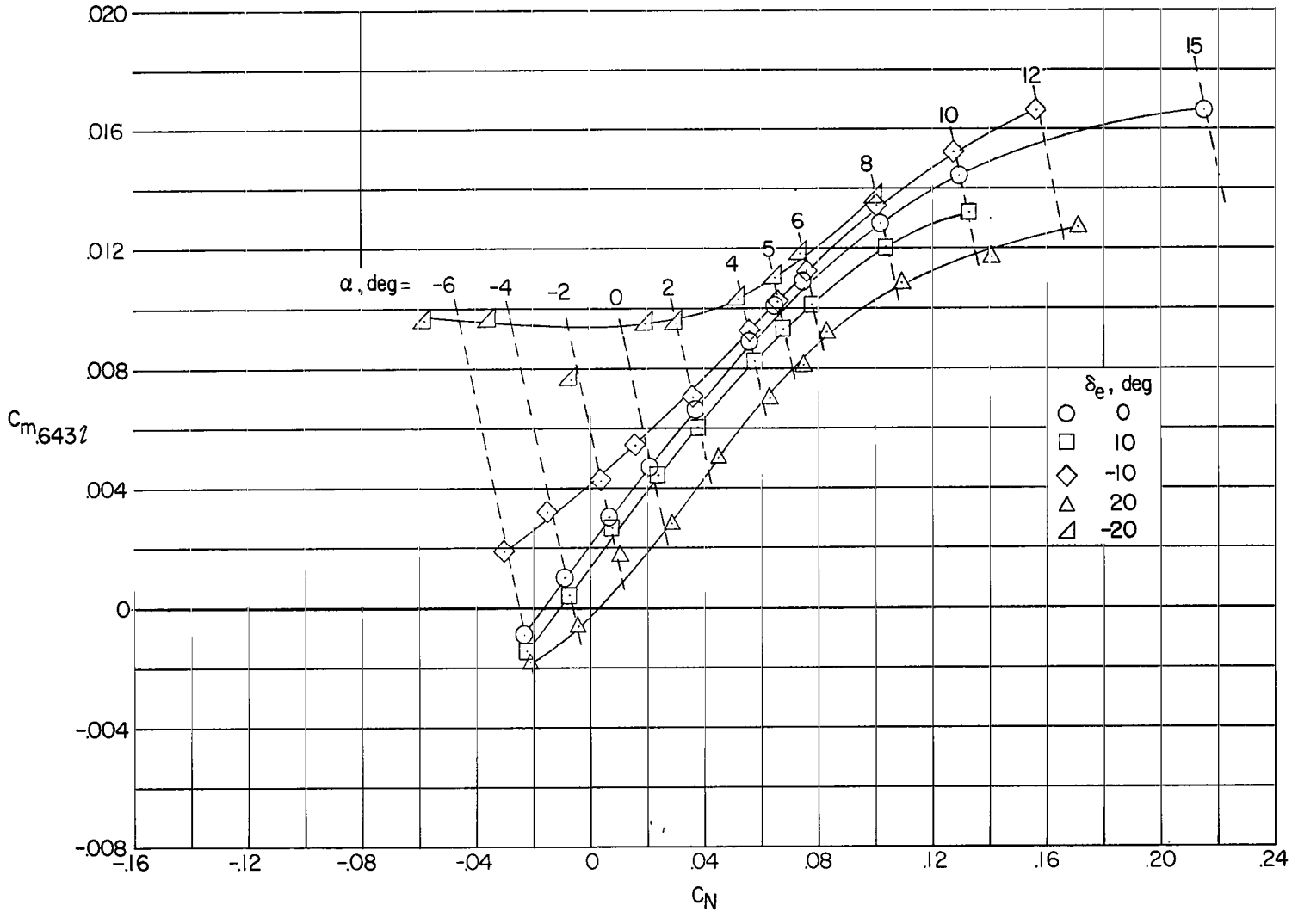

(b) Stability.

Figure 3.- Concluded.

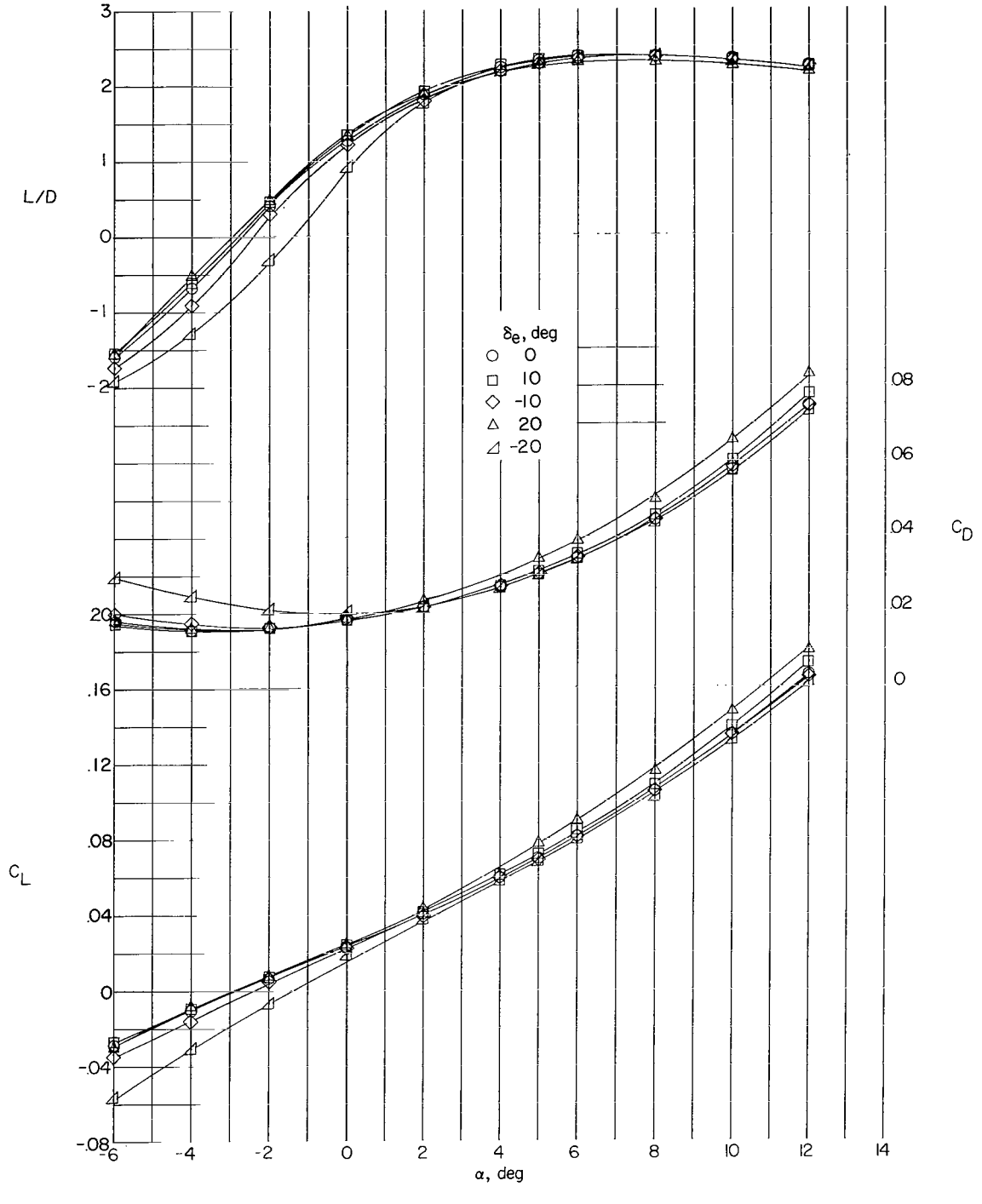

(a) Performance.

Figure 4.- Longitudinal stability and performance of configuration $N_1B_1W_2$.

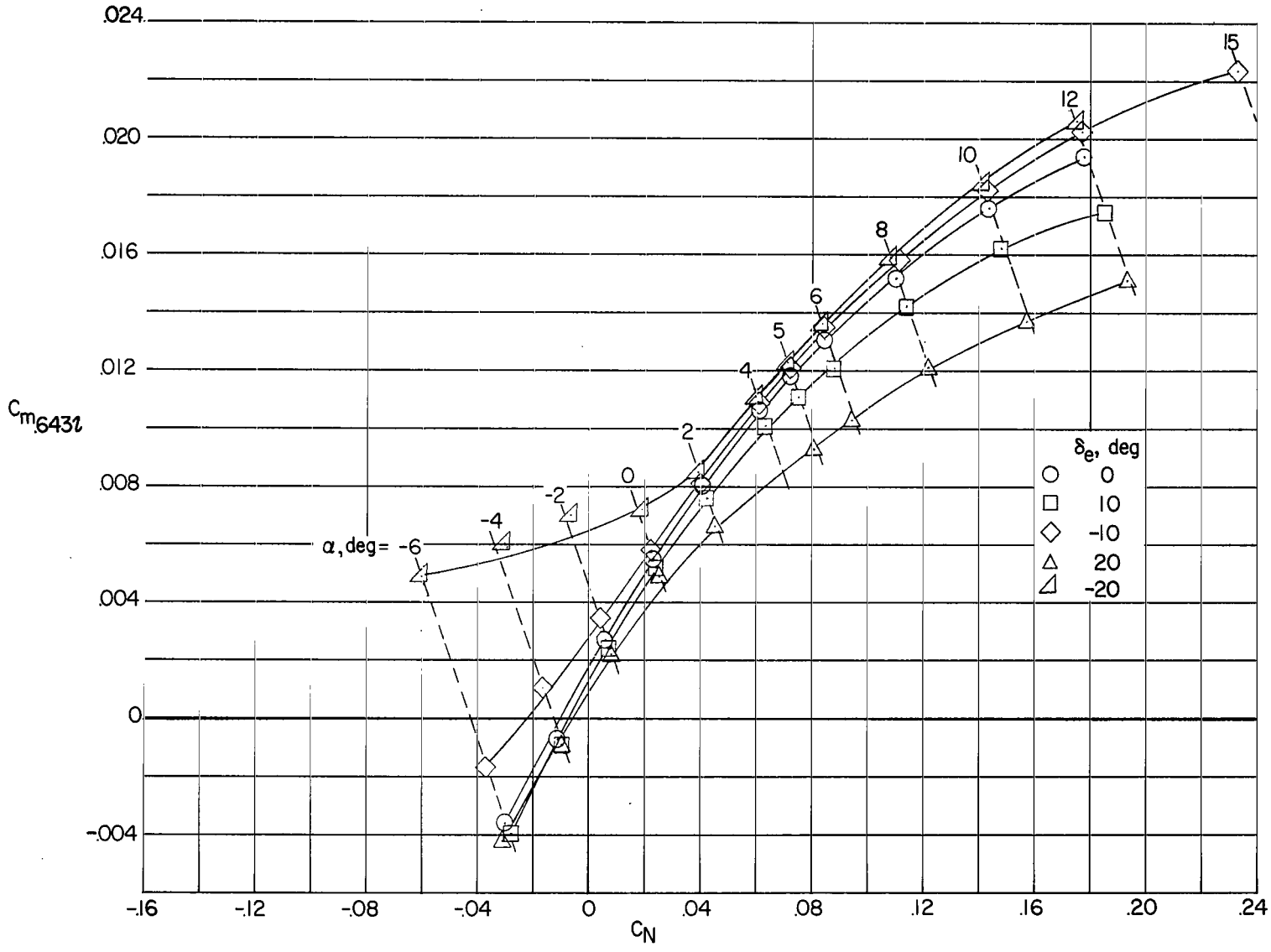

(b) Stability.

Figure 4.- Concluded.

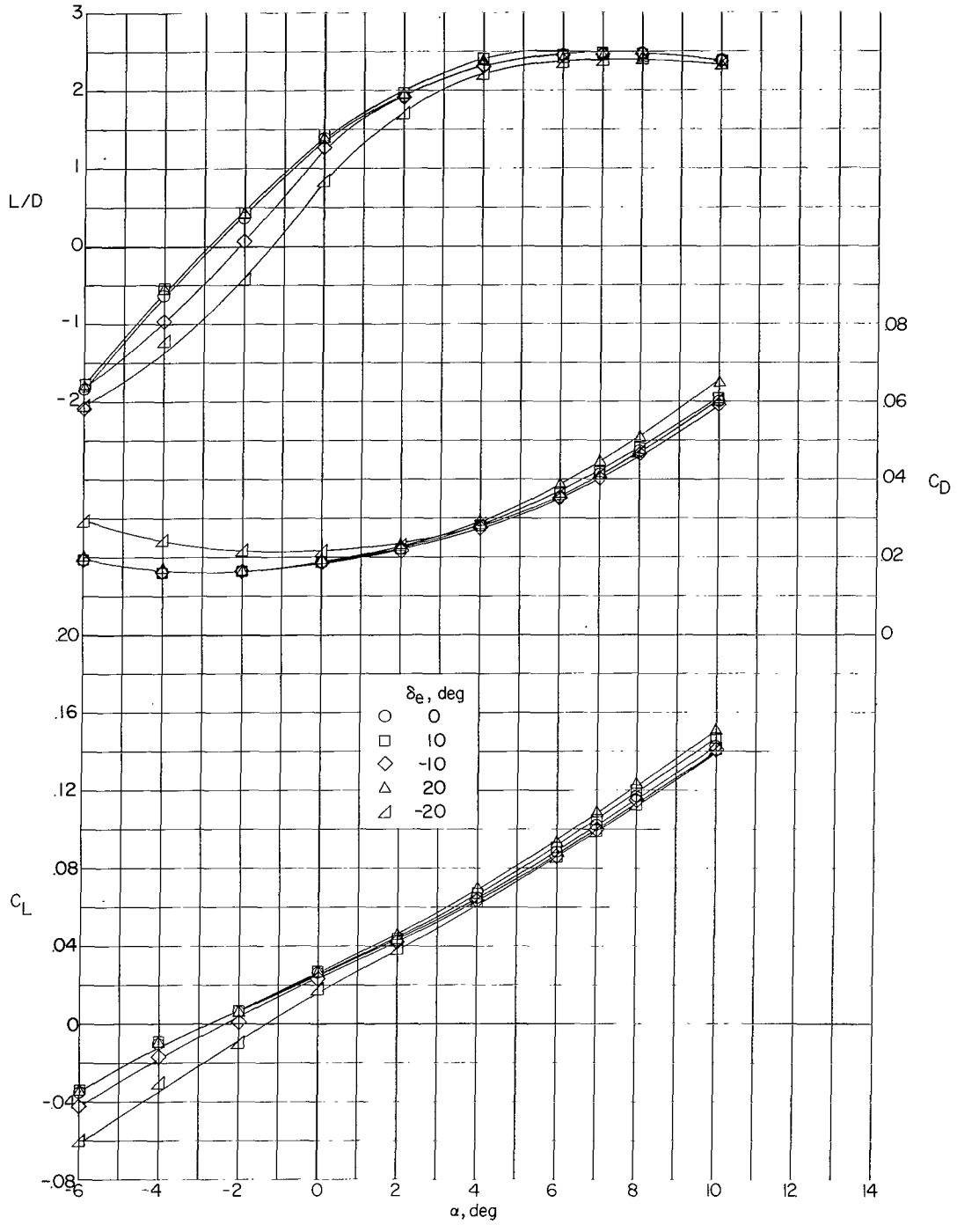

(a) Performance.

Figure 5.- Longitudinal stability and performance of configuration $N_1B_1W_3$.

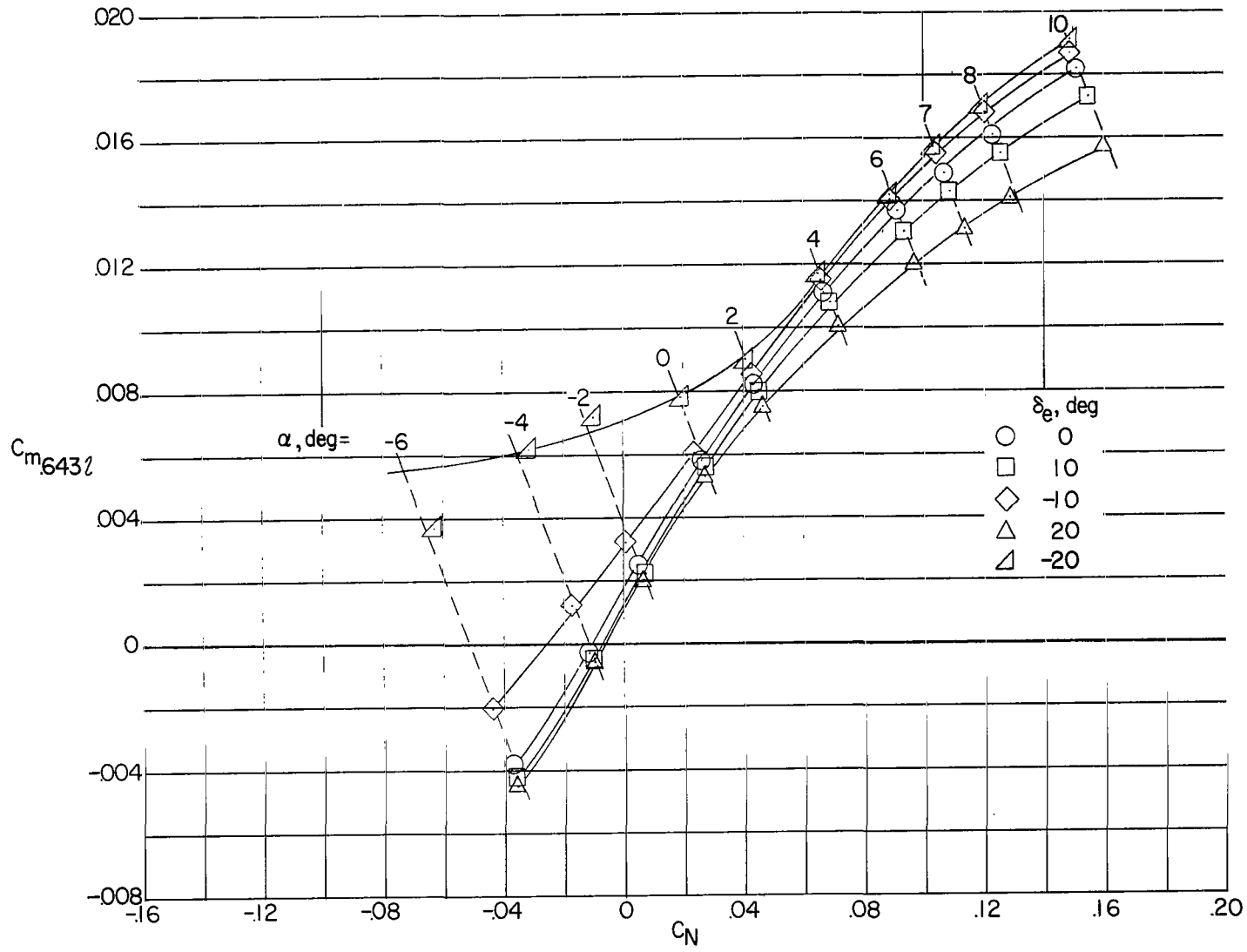

(b) Stability.

Figure 5.- Concluded.

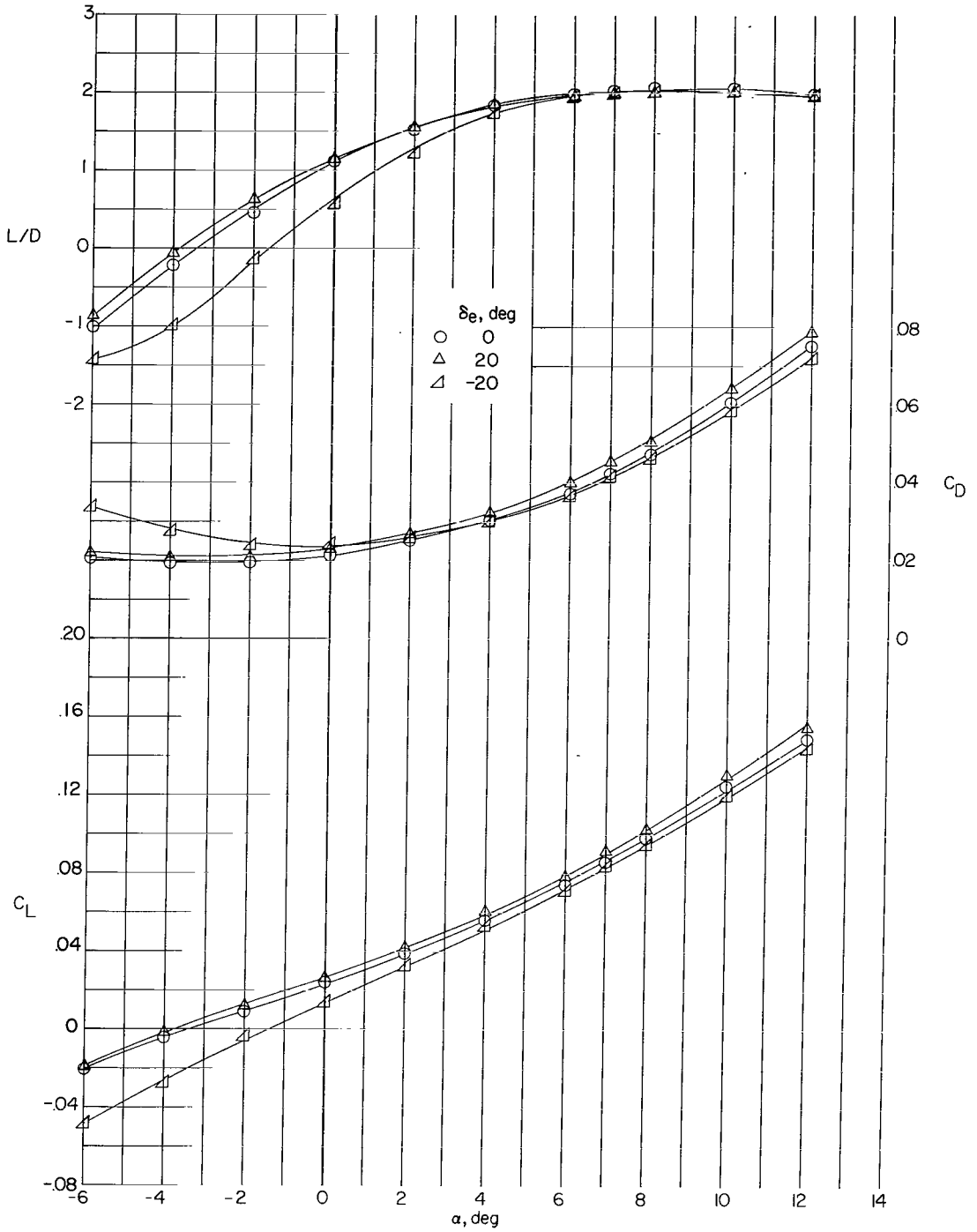

(a) Performance.

Figure 6.- Longitudinal stability and performance of configuration $N_2B_1W_1$.

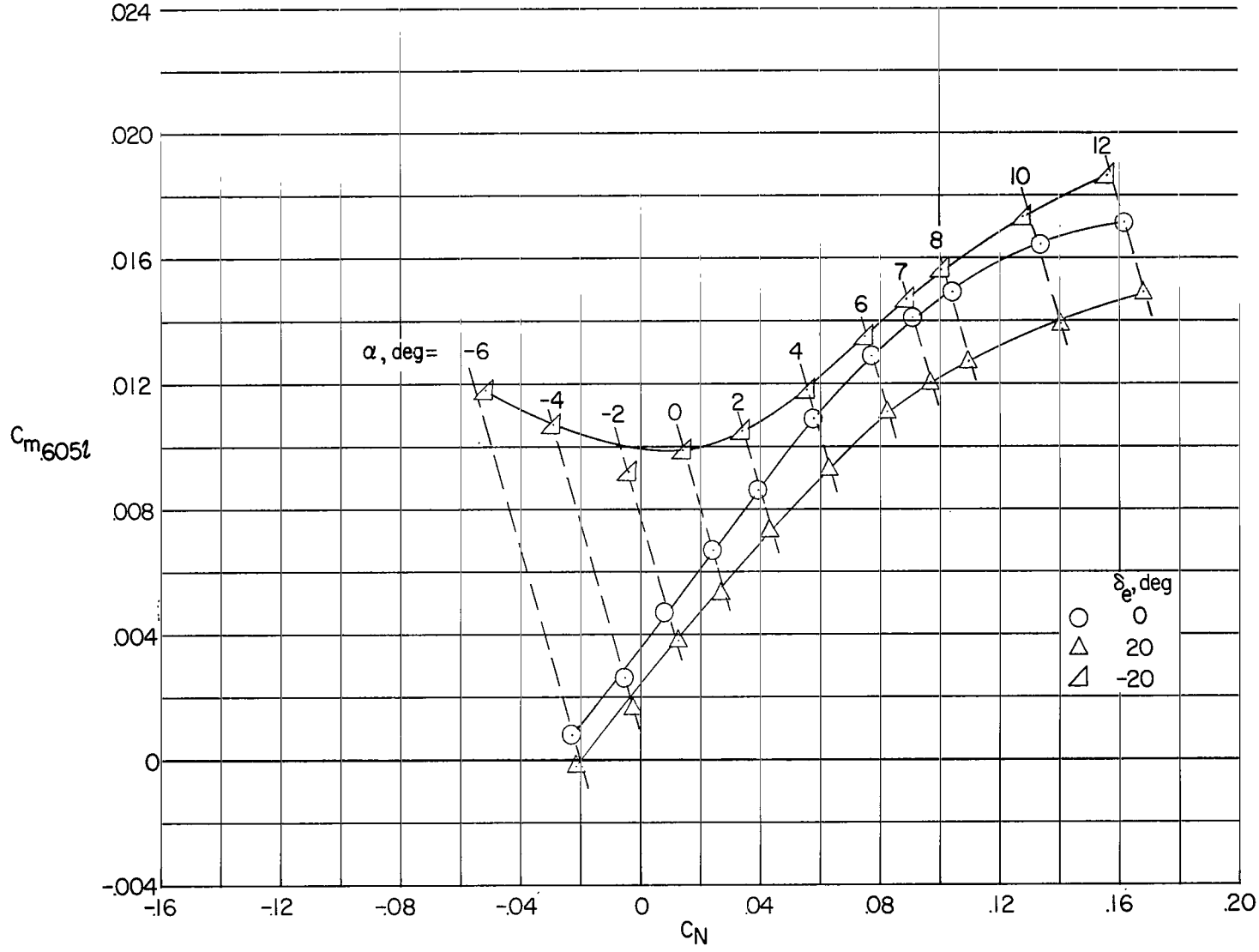

(b) Stability.

Figure 6.- Concluded.

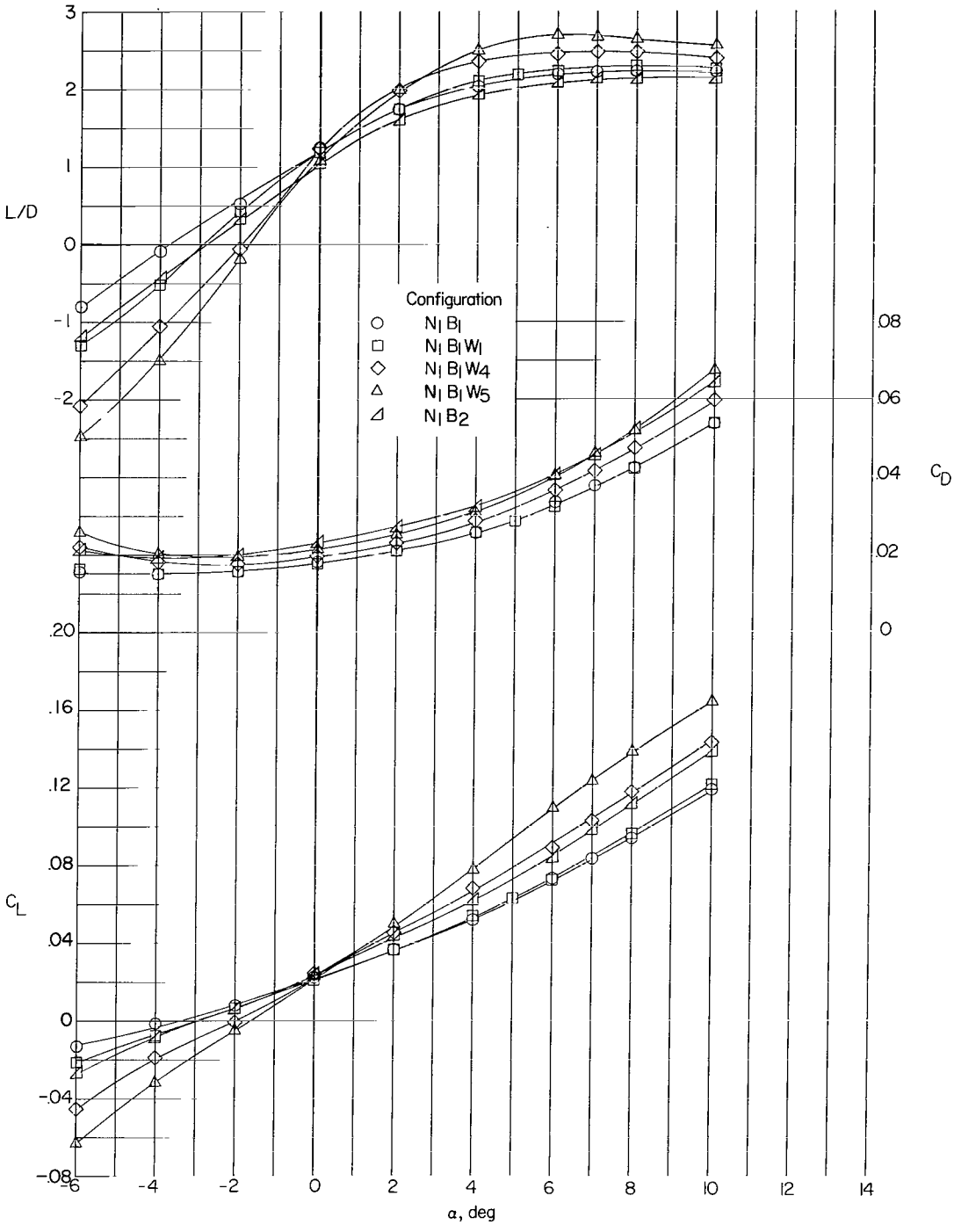

(a) Performance.

Figure 7.- Effect of wing size and body volume on stability and performance.

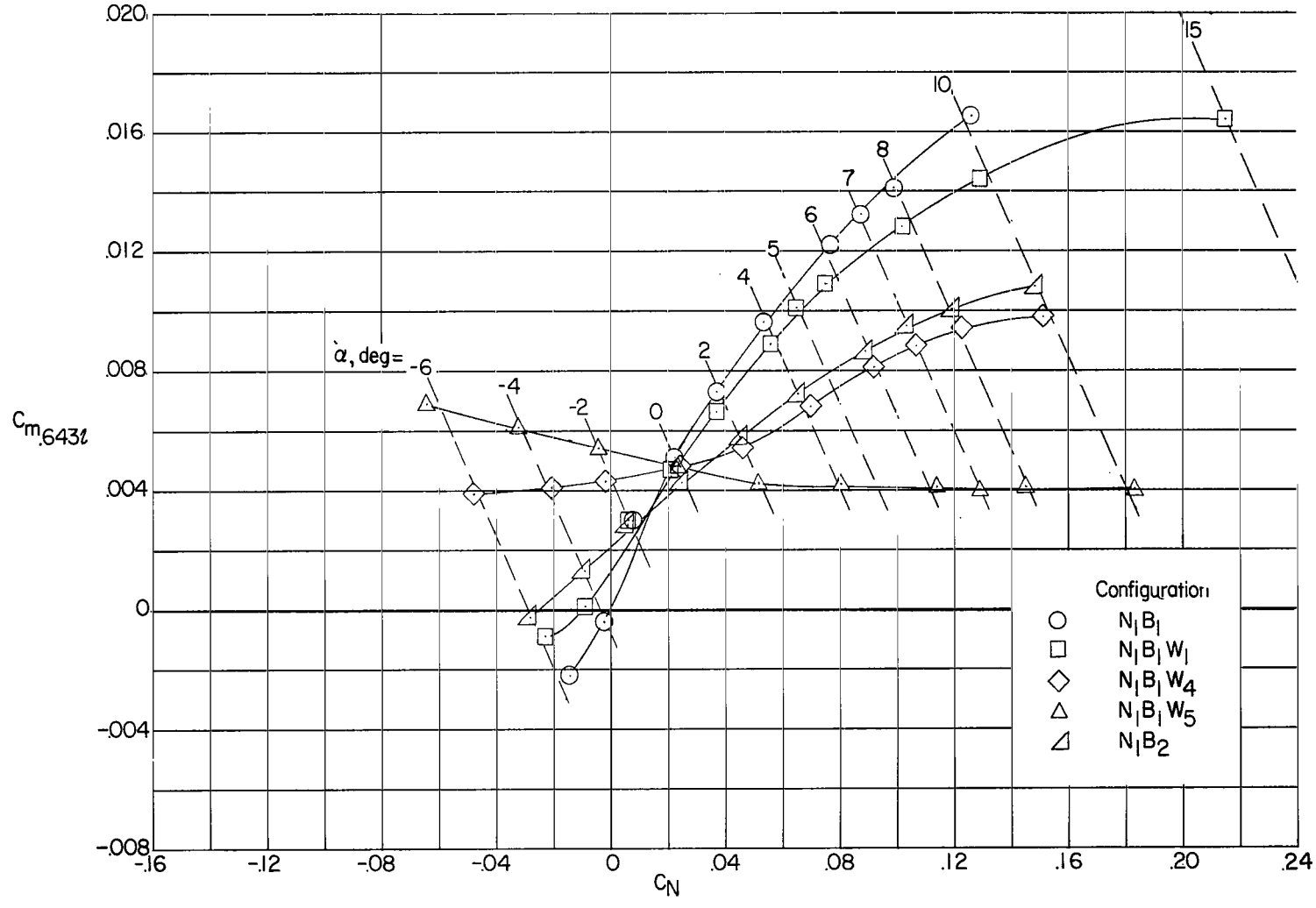

(b) Stability.

Figure 7.- Concluded.

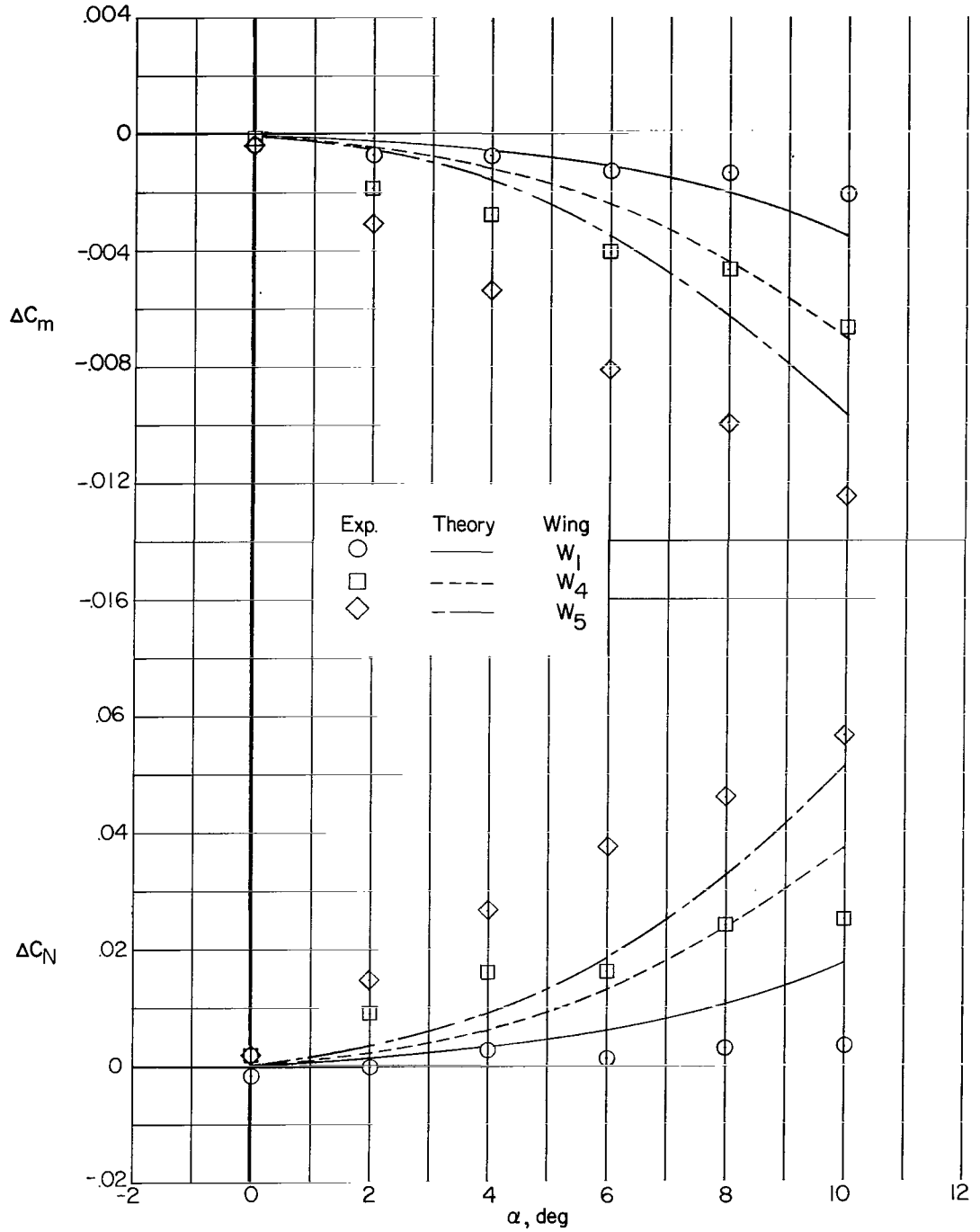

(a) Variation with angle of attack.

Figure 8.- Theoretical and experimental wing contribution to C_N and C_m.

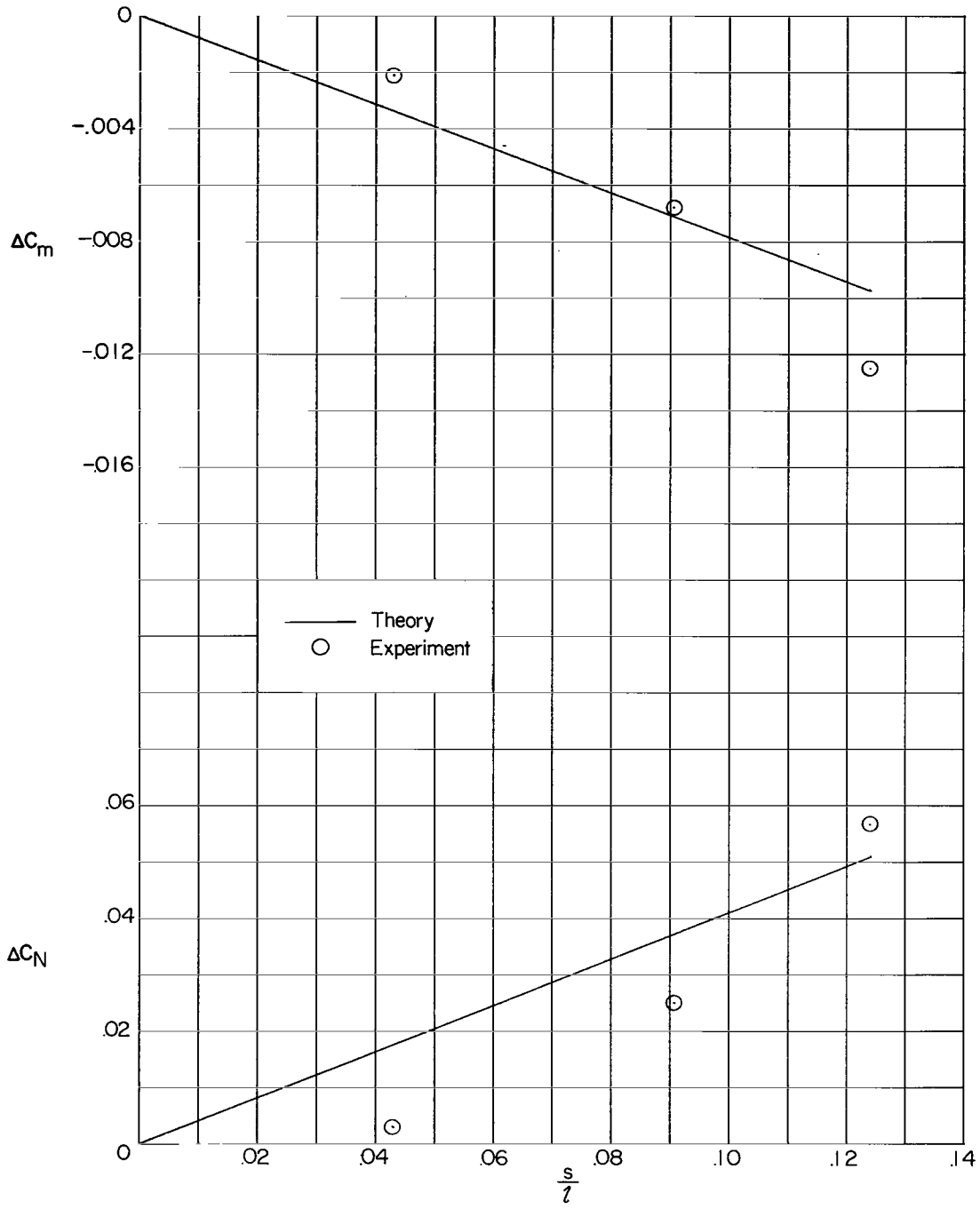

(b) Variation with exposed semispan; $\alpha = 10^0$.

Figure 8.- Concluded.

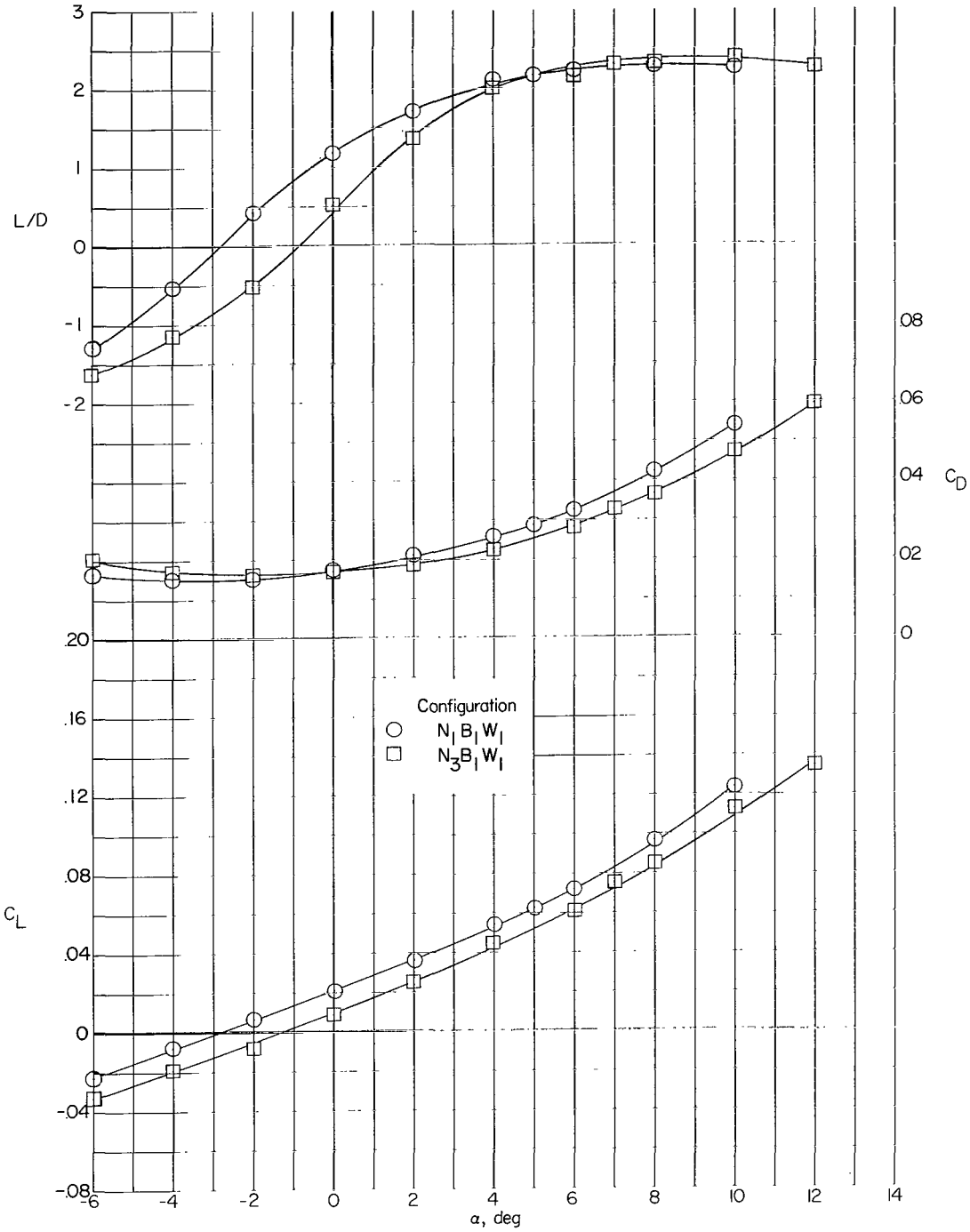

(a) Performance.

Figure 9.- Effect of nose cant on stability and performance. Reference length, 15.000 in. (38.10 cm).

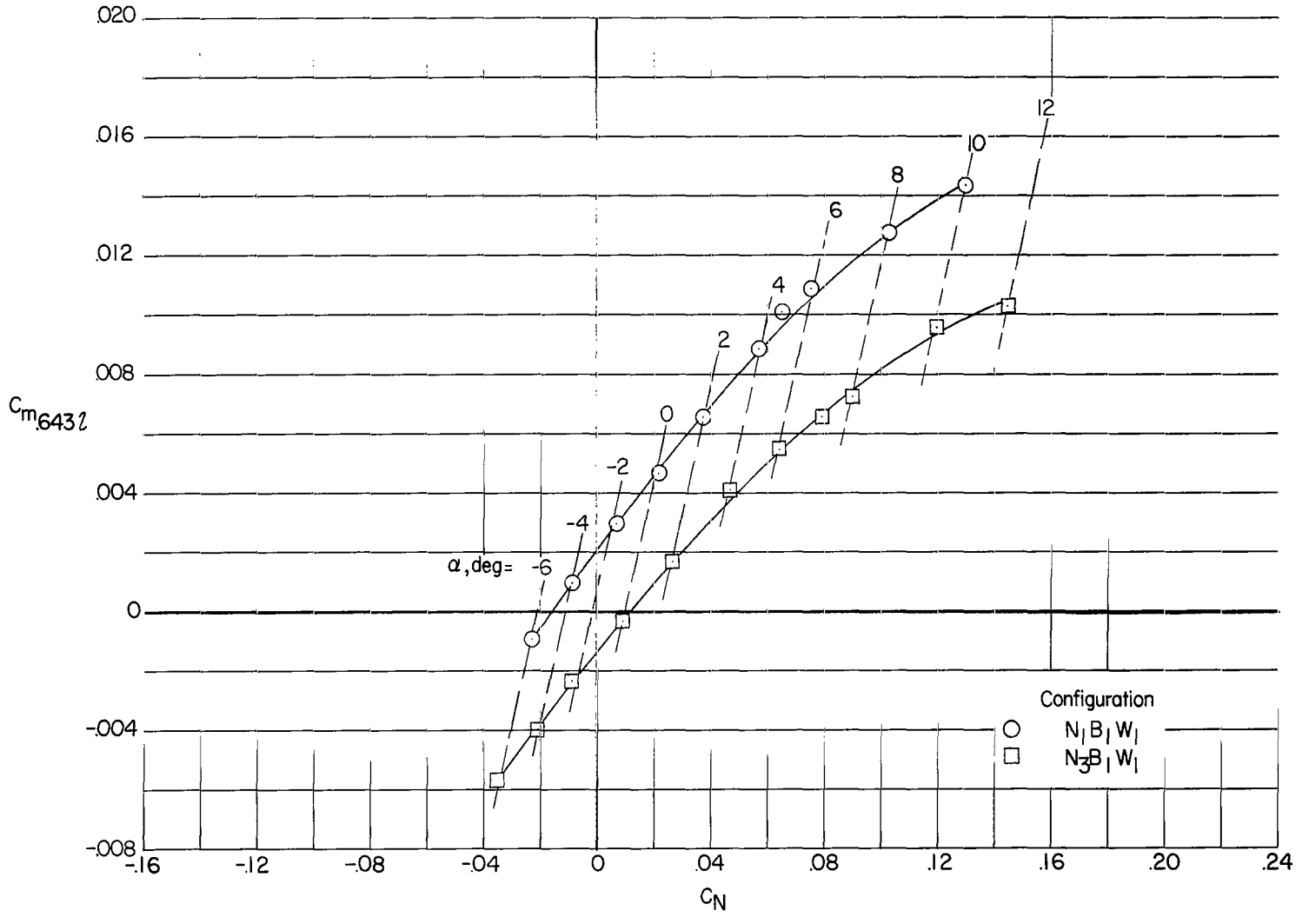

(b) Stability.

Figure 9.- Concluded.

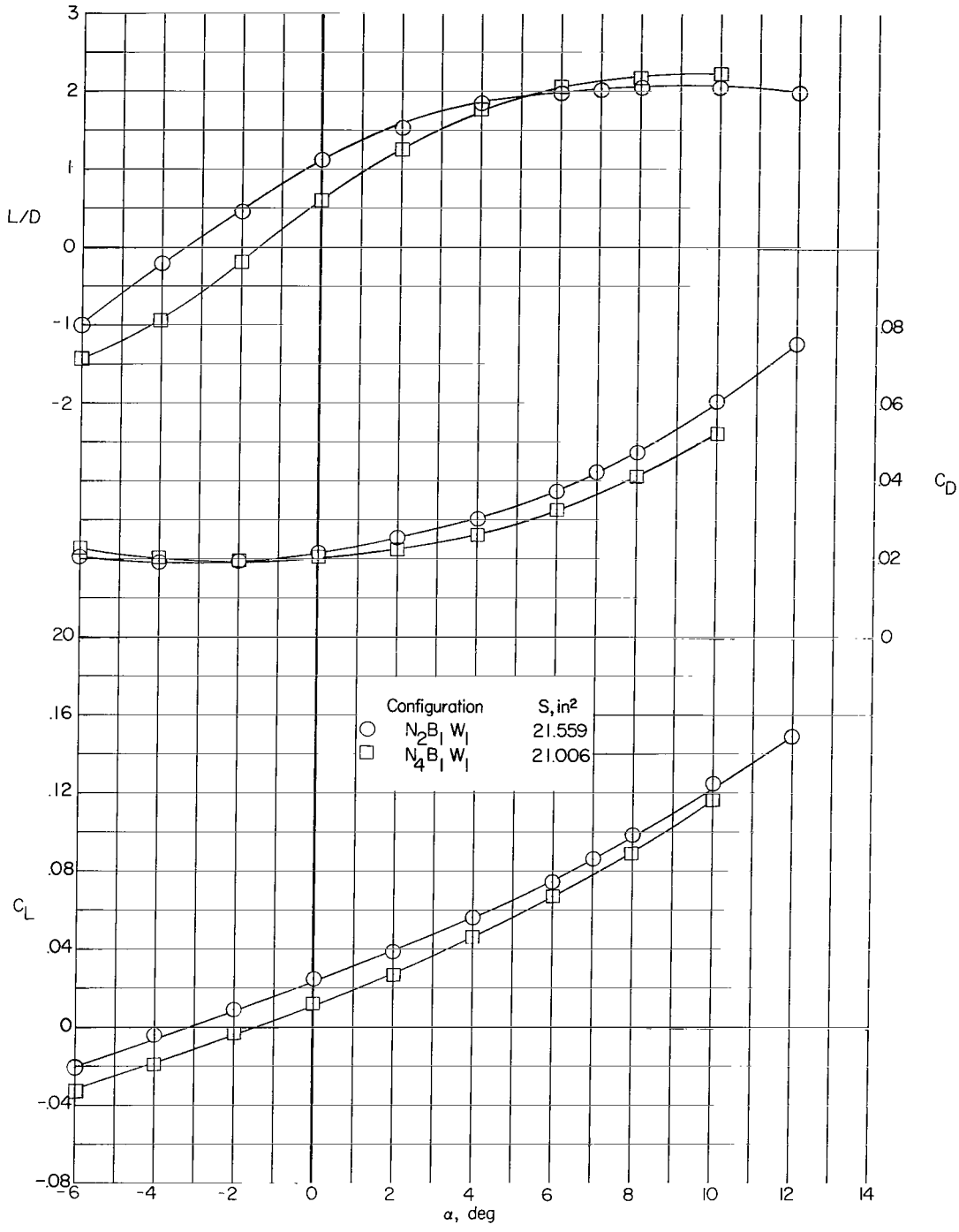

(a) Performance.

Figure 10.- Effect of nose cant on stability and performance. Reference length, 13.572 in. (34.47 cm).

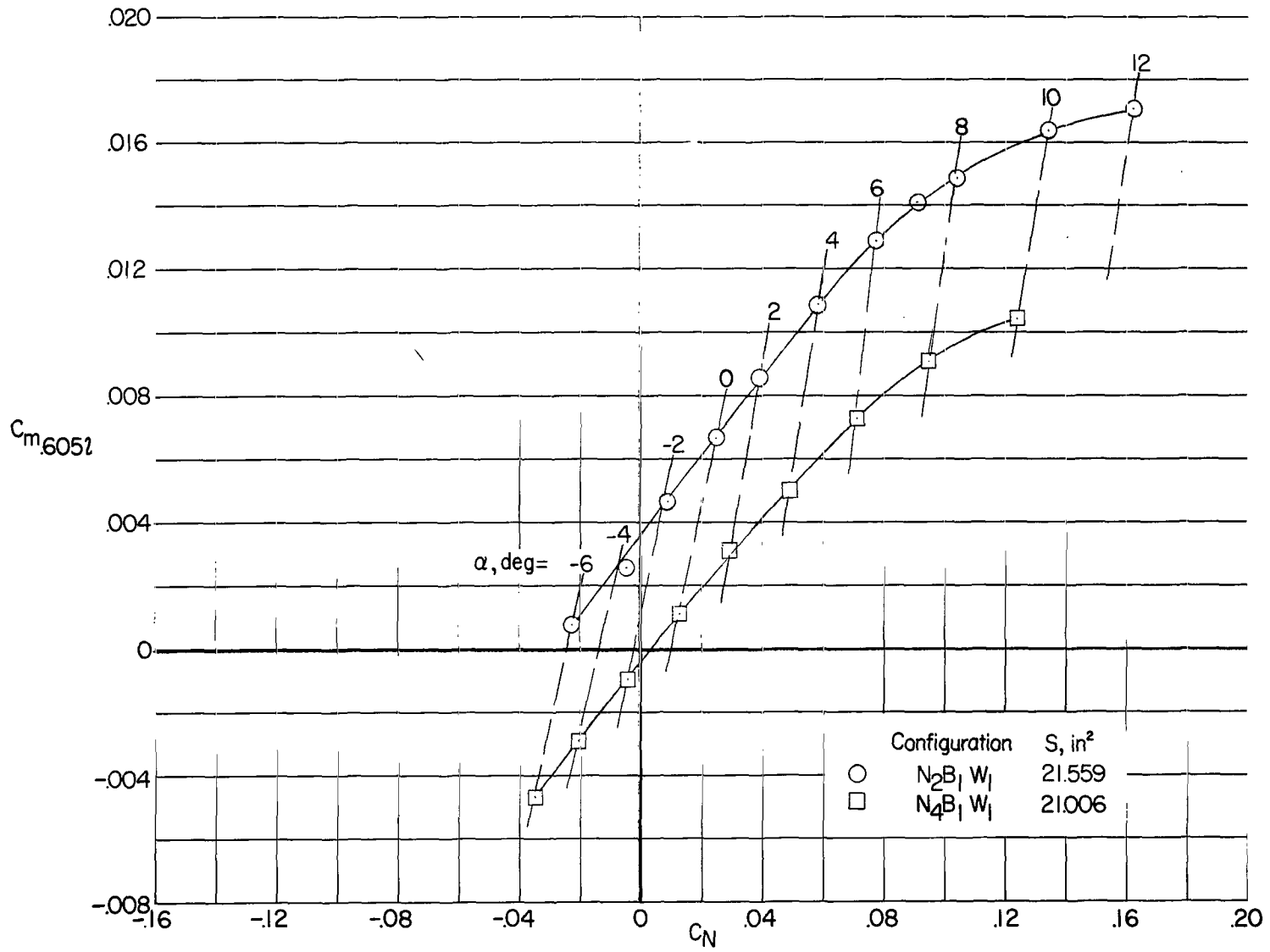

(b) Stability.

Figure 10.- Concluded.

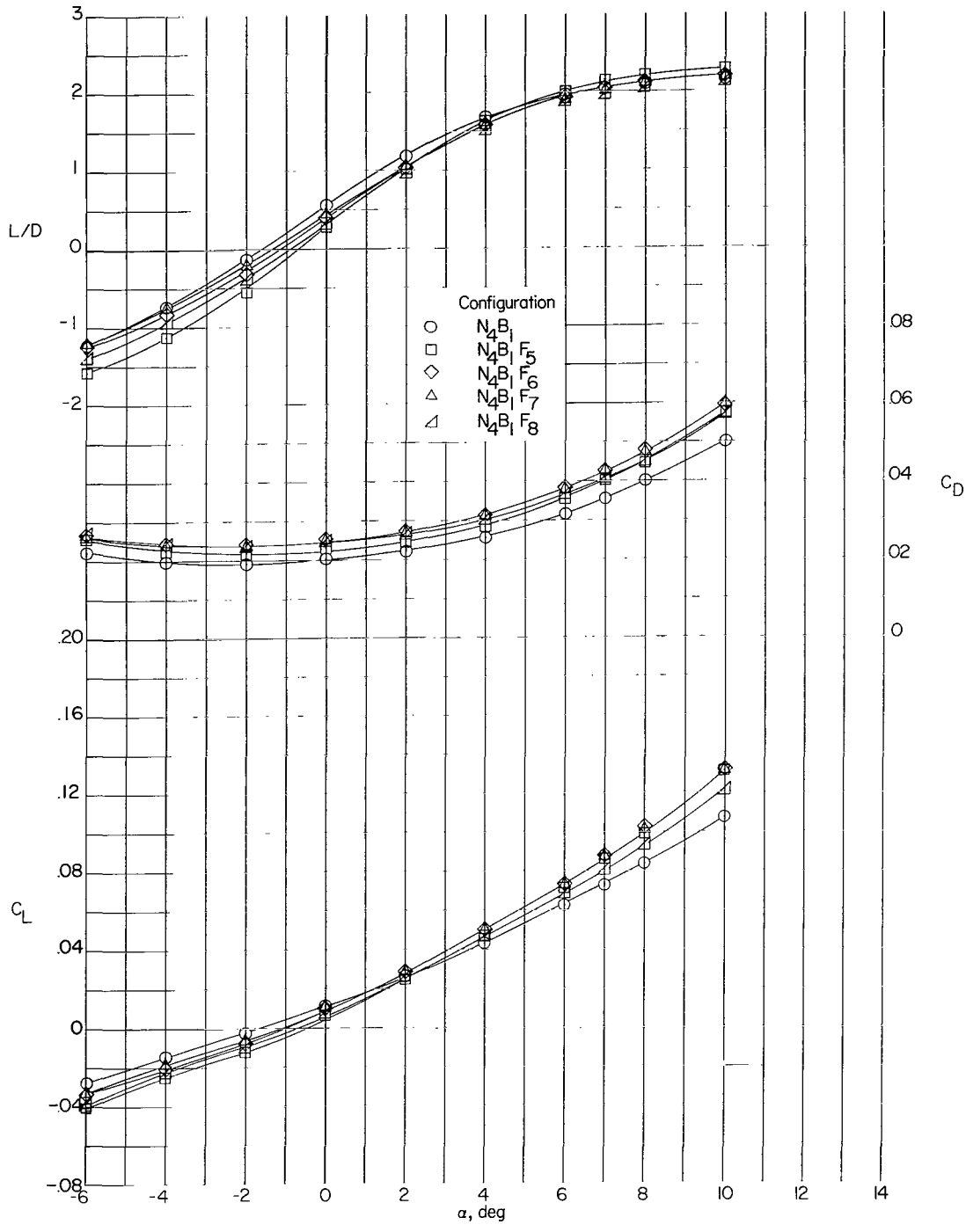

(a) Performance.

Figure 11.- Effect of ventral fin on the stability and performance of configuration N_4B_1.

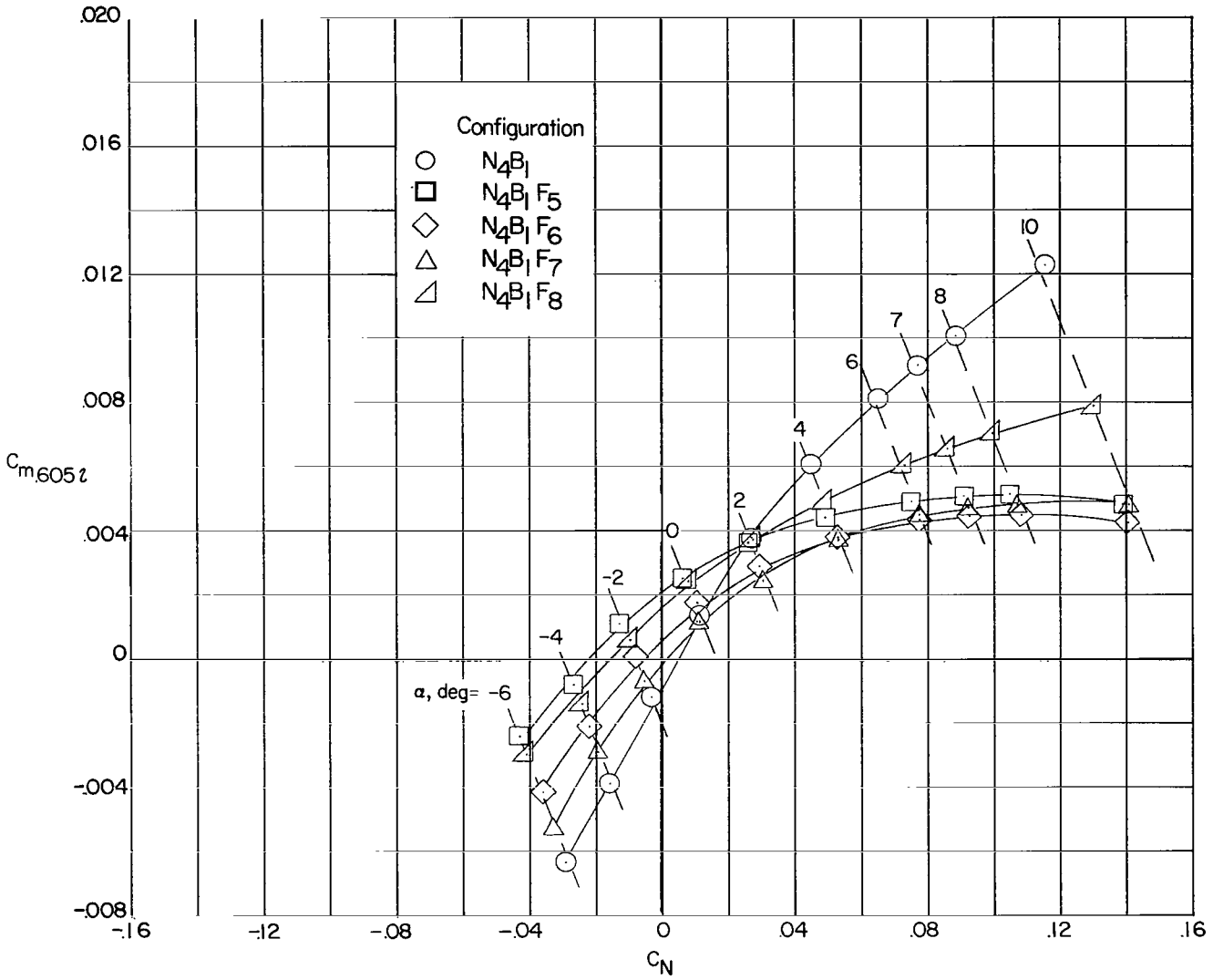

(b) Longitudinal stability.

Figure 11.- Continued.

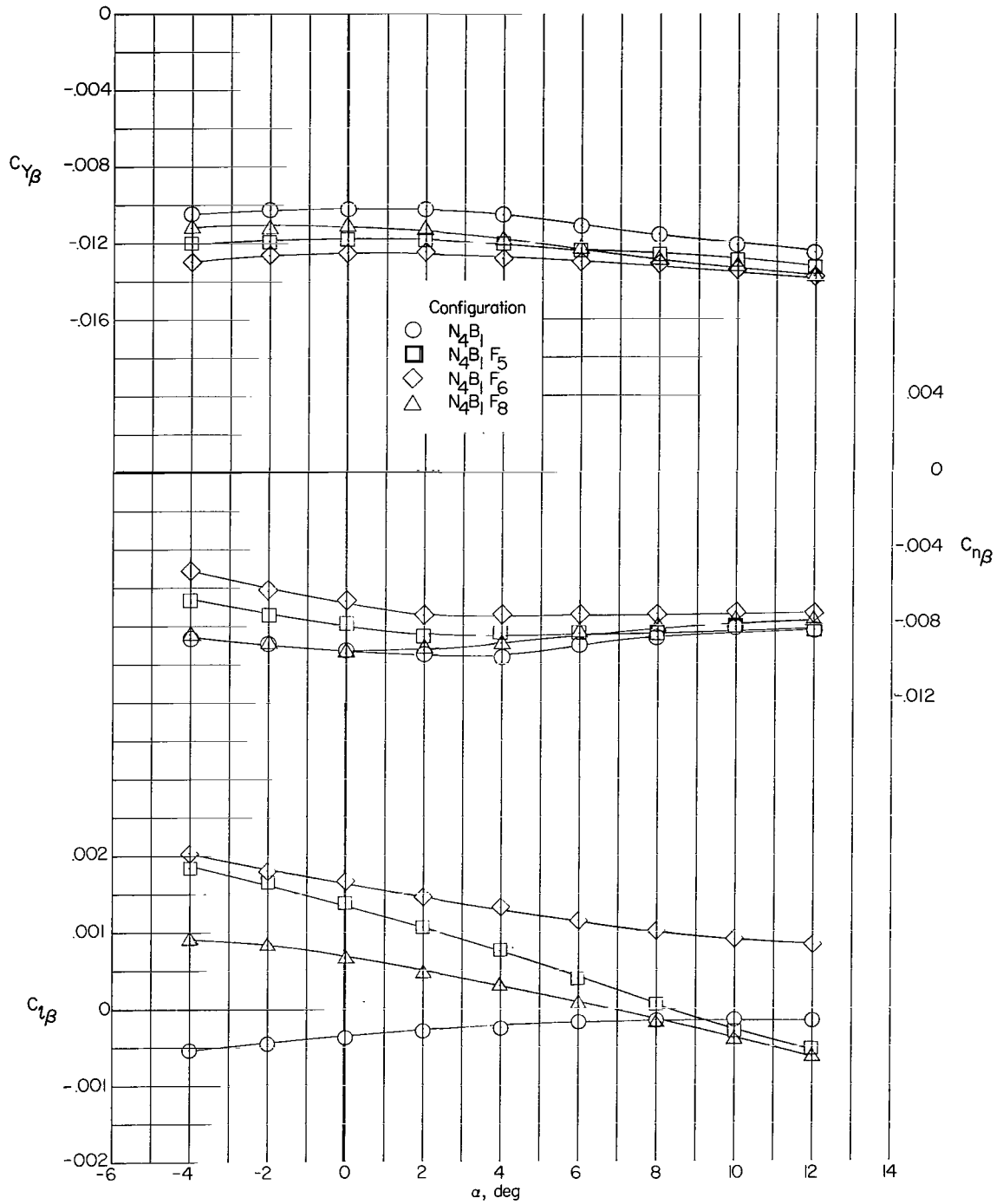

(c) Lateral and directional stability.

Figure 11.- Concluded.

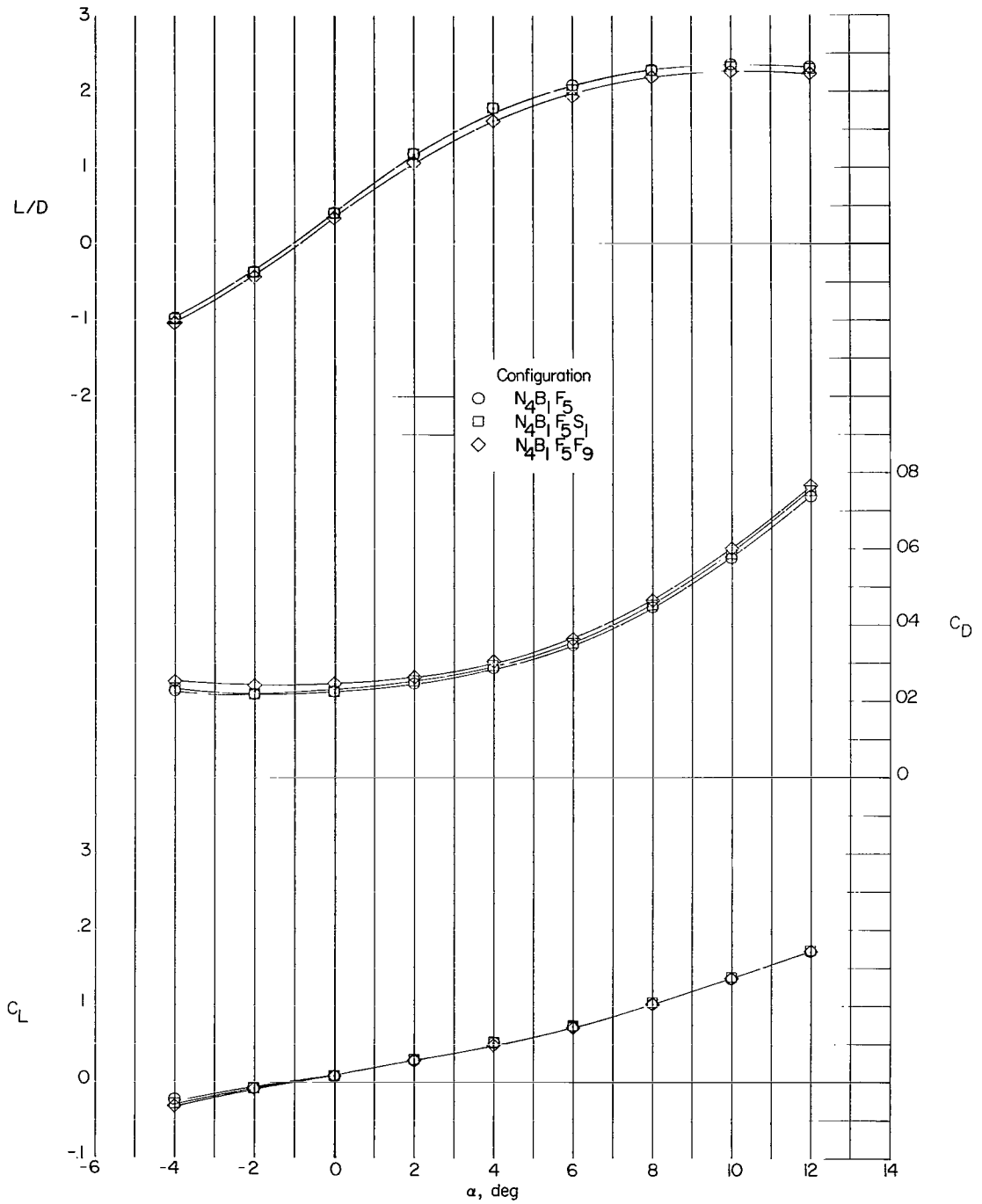

(a) Performance.

Figure 12.- Effect of fin F_1 and strake S_1 on the stability and performance of configuration $N_4B_1F_5$.

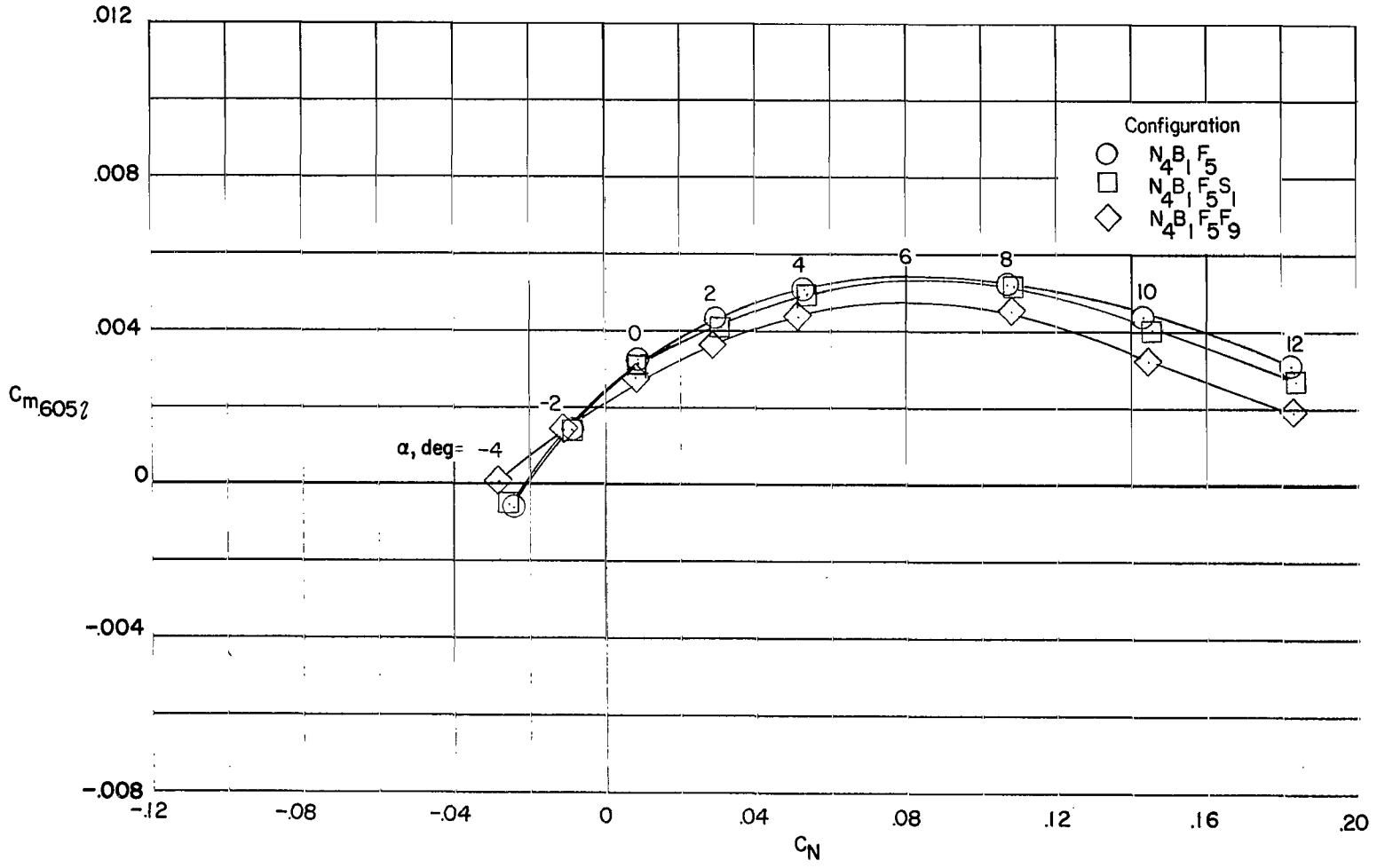

(b) Longitudinal stability.

Figure 12.- Continued.

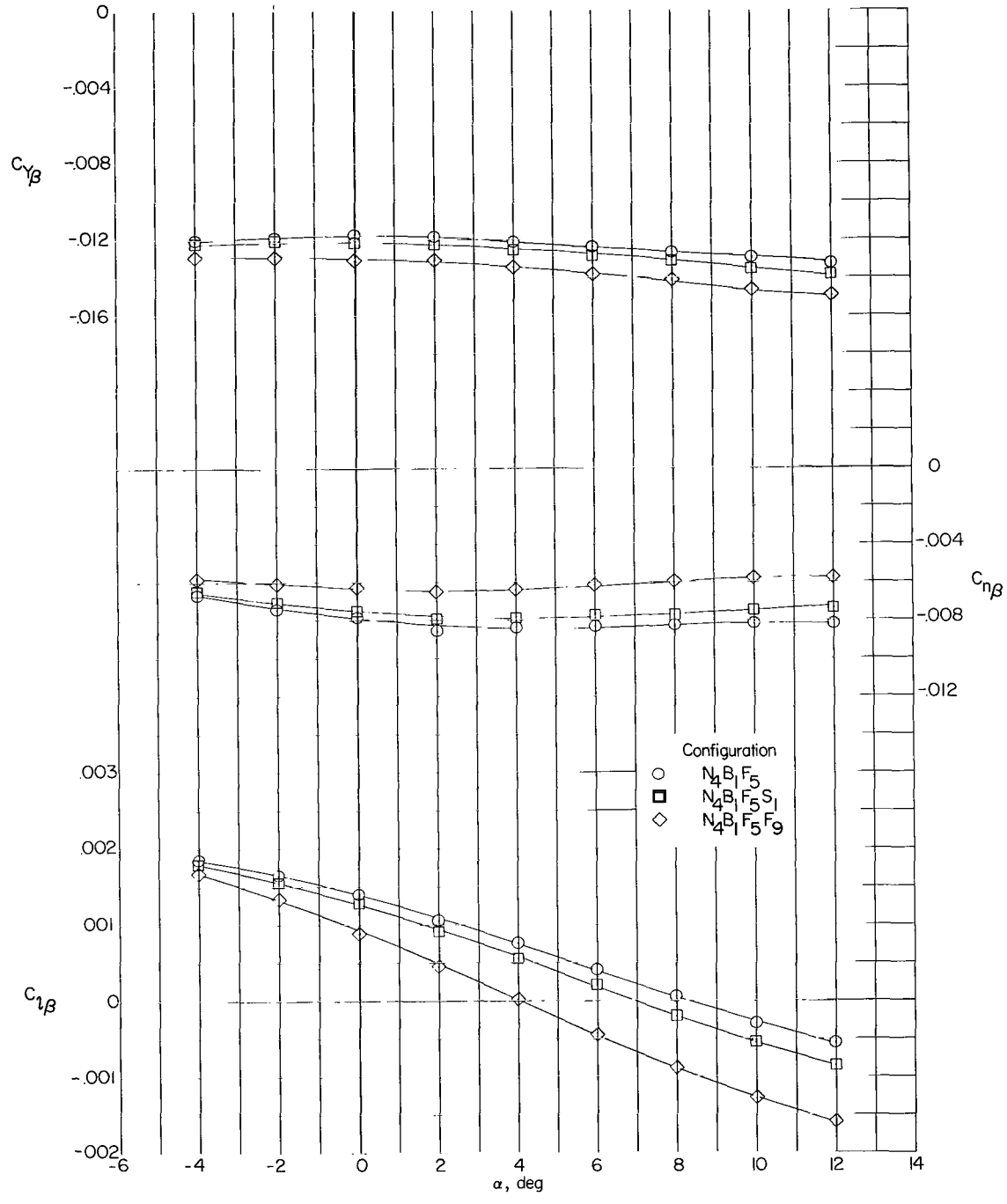

(c) Lateral and directional stability.

Figure 12.- Concluded.

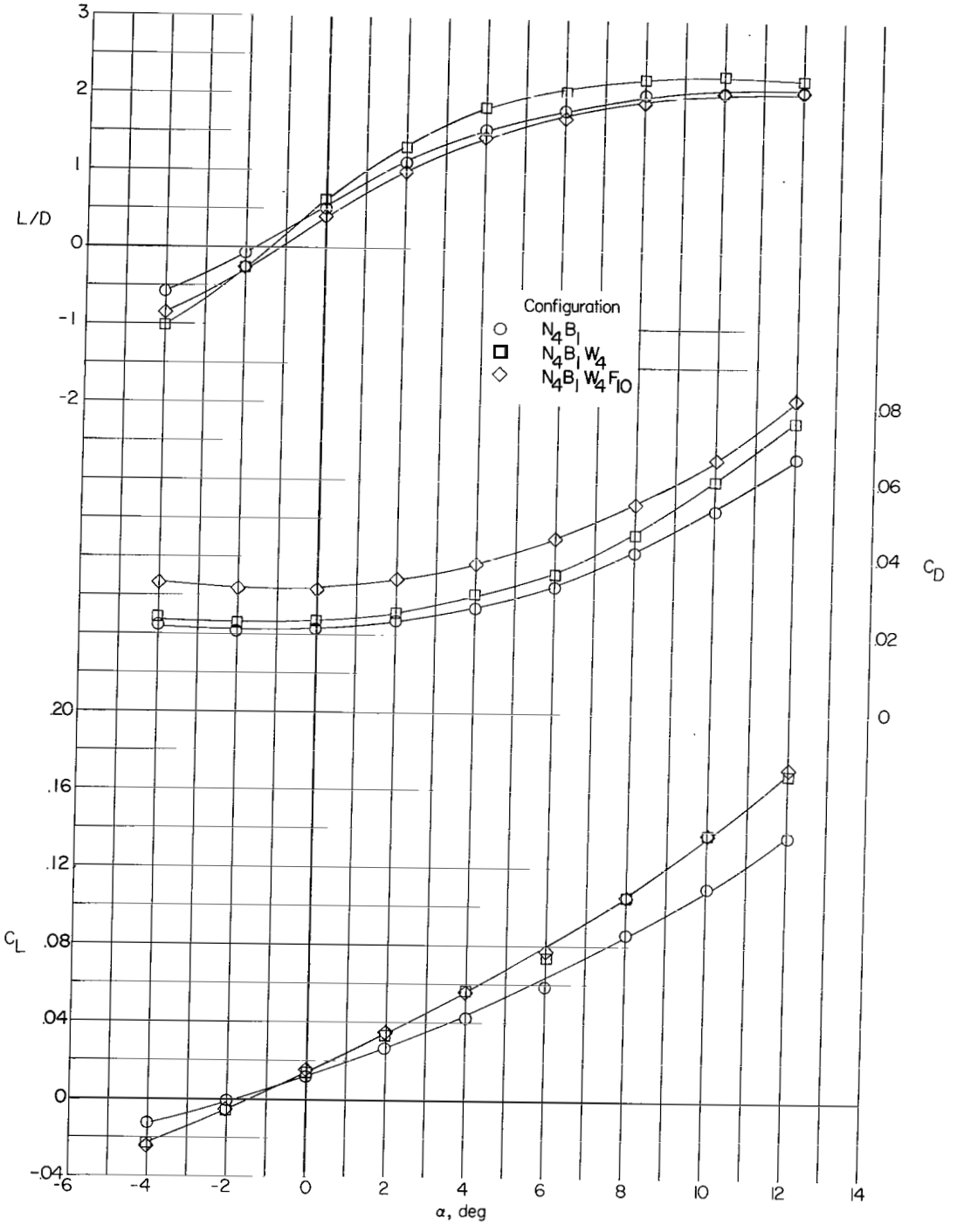

(a) Performance.

Figure 13.- Effect of wing and tip fins on the stability and performance of configuration N_4B_1.

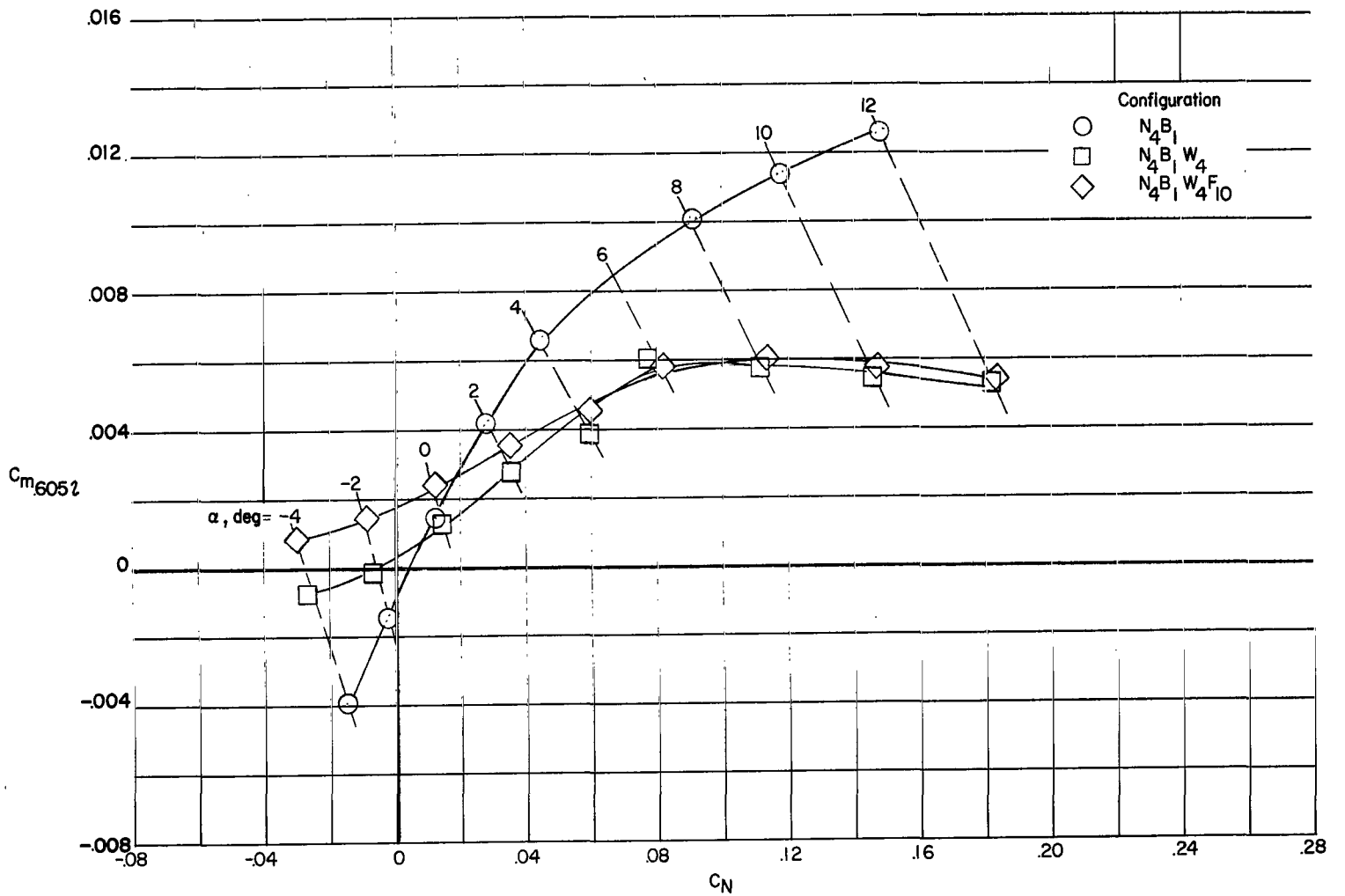

(b) Longitudinal stability.

Figure 13.- Continued.

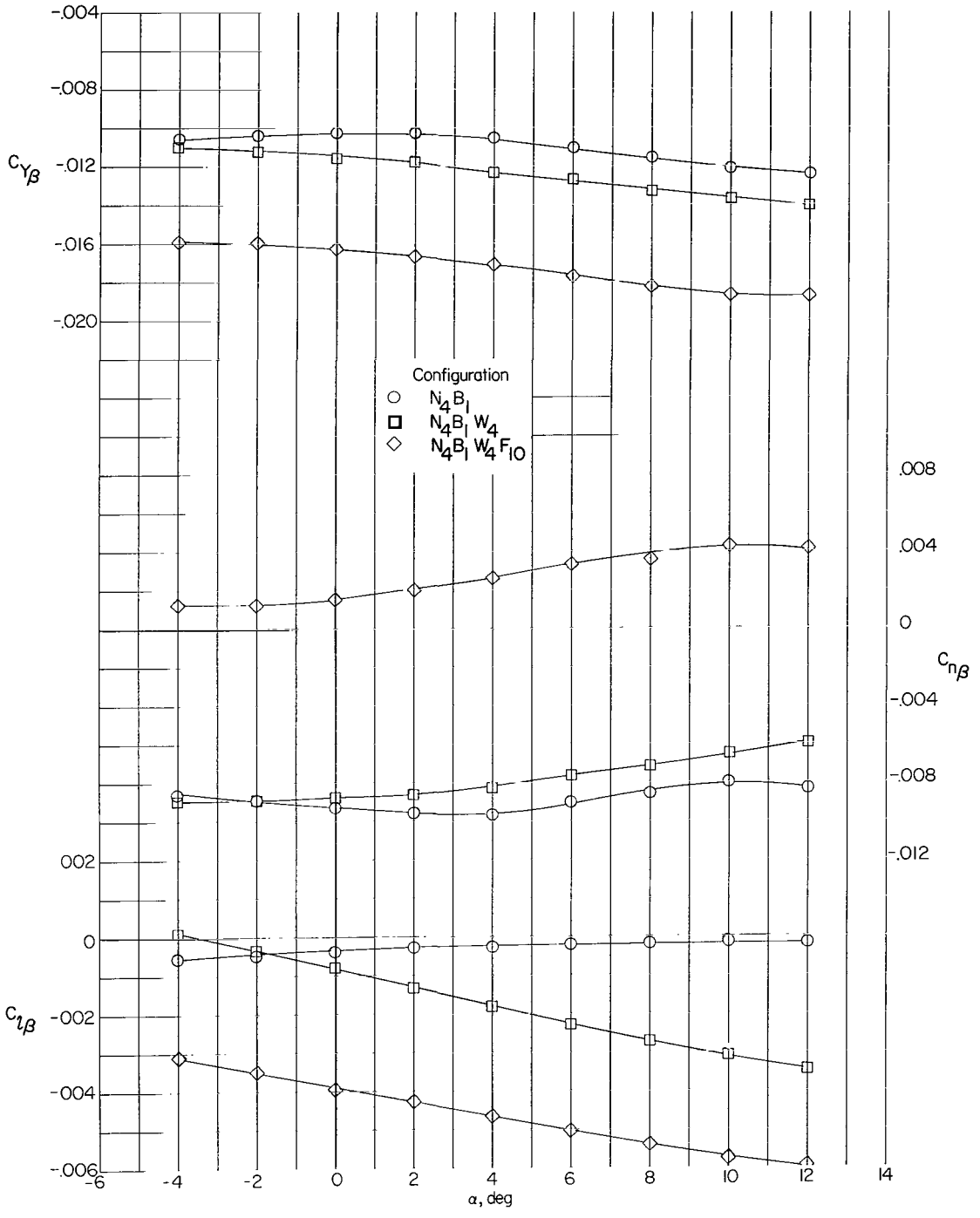

(c) Lateral and directional stability.

Figure 13.- Concluded.

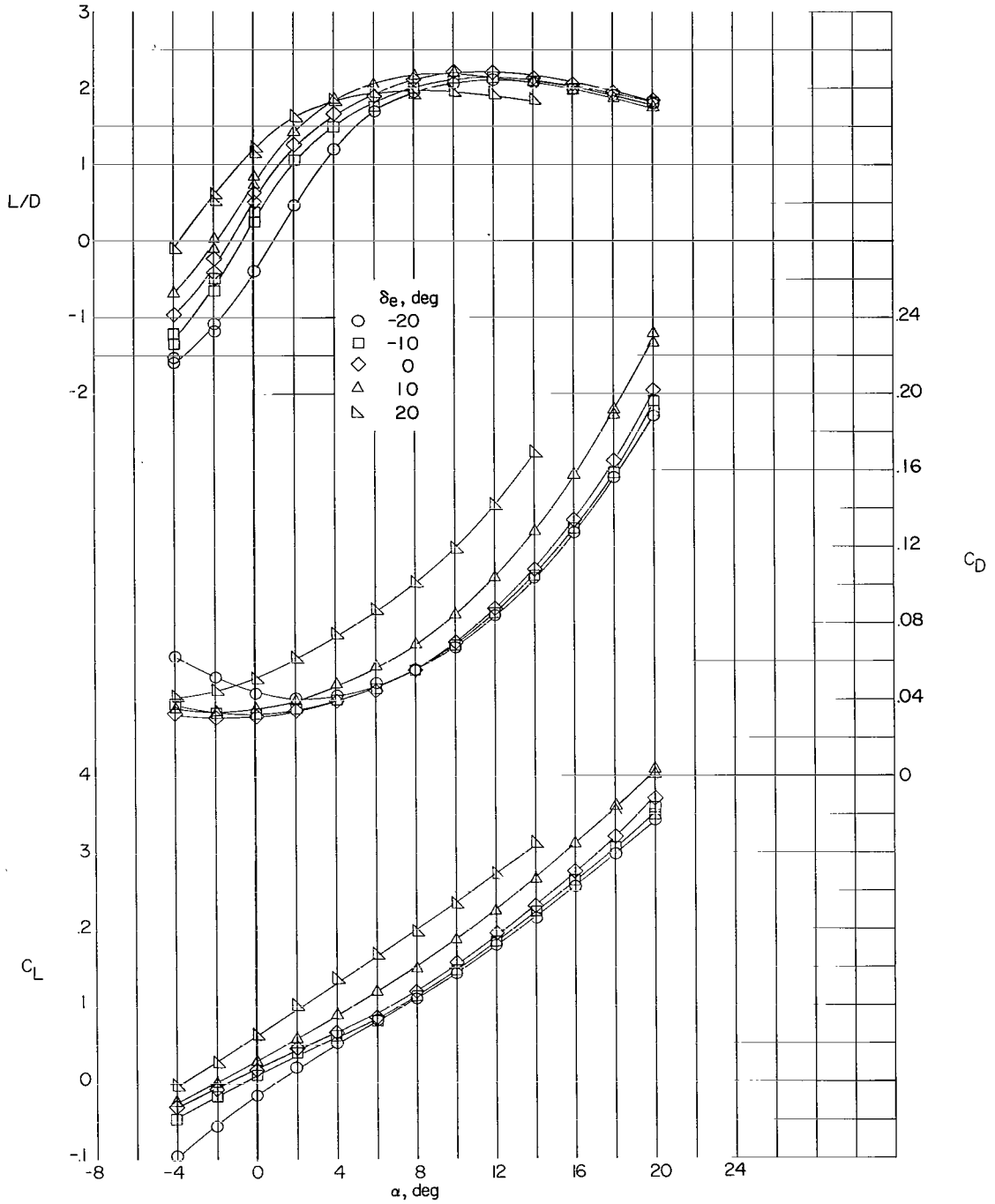

(a) Performance.

Figure 14.- Longitudinal characteristics of configuration $N_4B_1W_4F_{11}$.

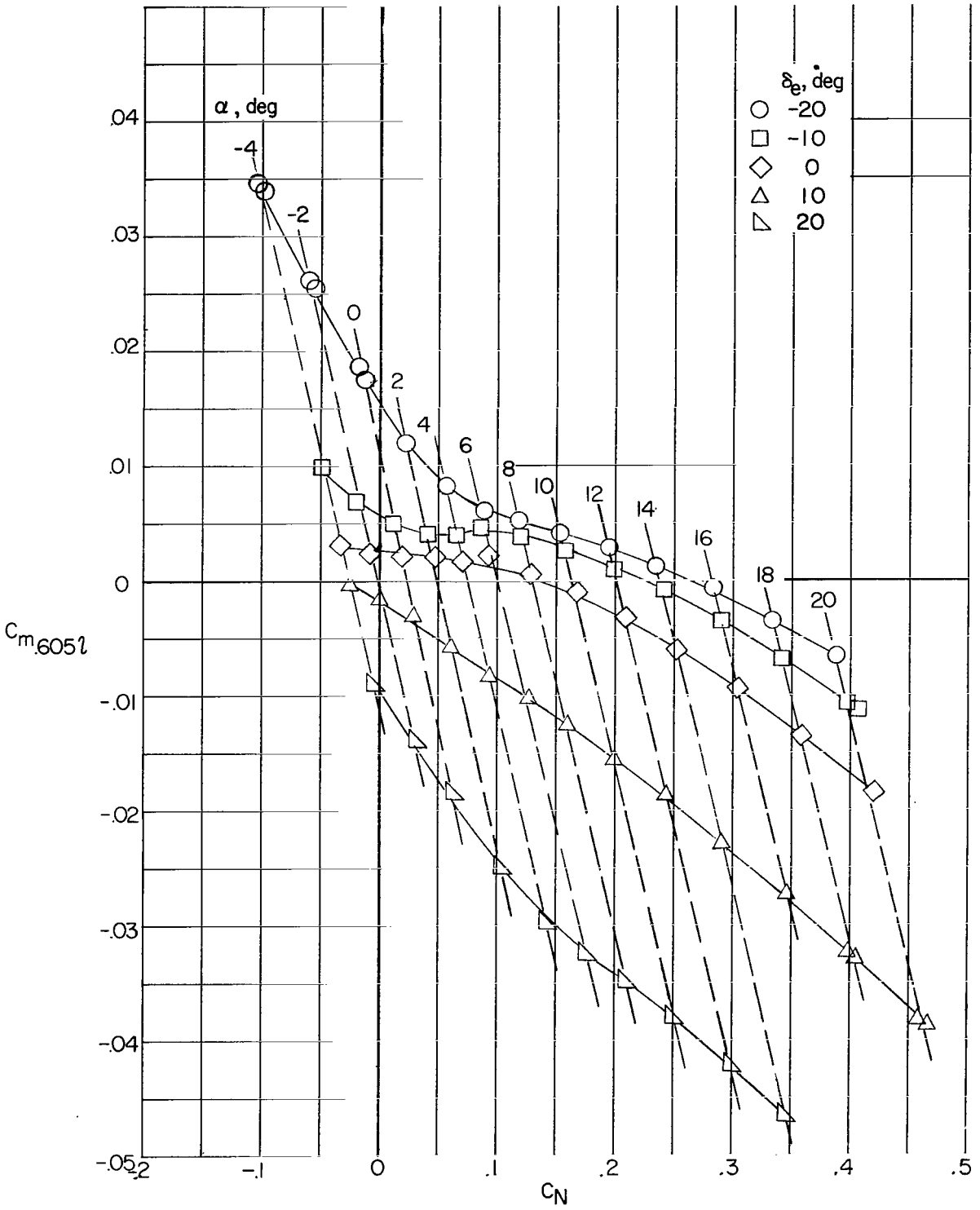

(b) Stability.

Figure 14.- Concluded.

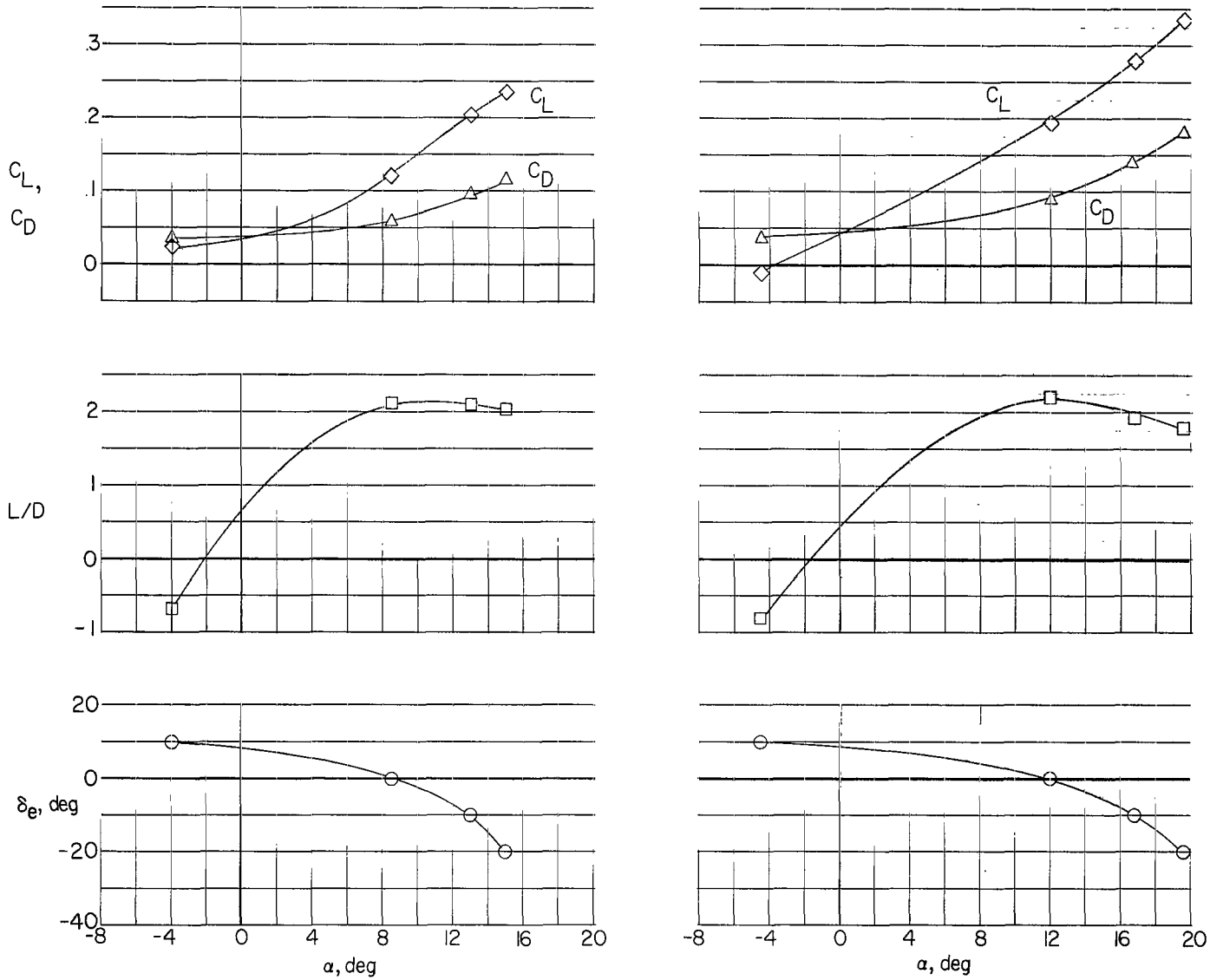

(a) Center of gravity at 0.605$\bar{l}$.

(b) Center of gravity at 0.621$\bar{l}$.

Figure 15.- A summary of the trimmed characteristics of configuration $N_4B_1W_4F_{11}$.

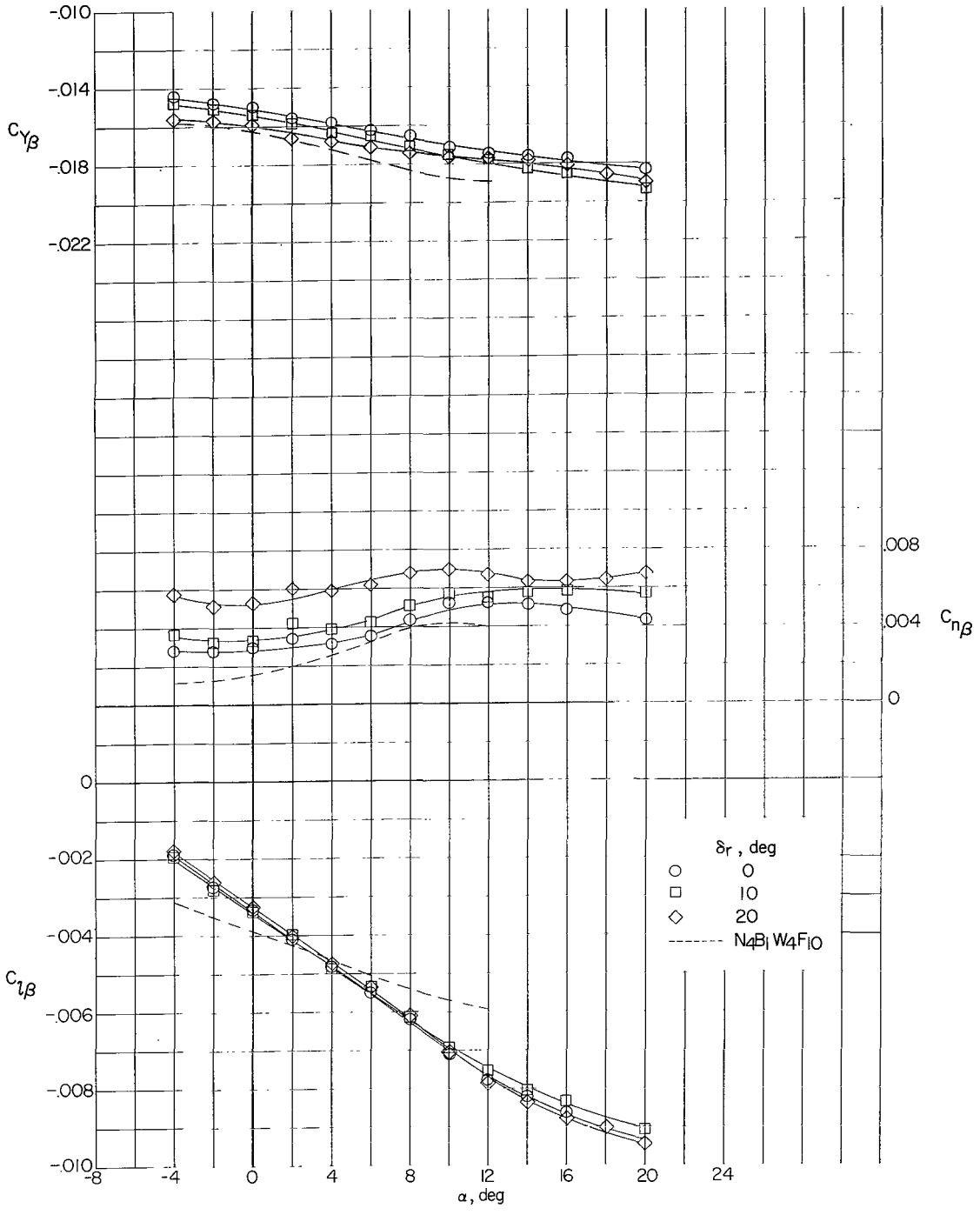

Figure 16.- Stability and control characteristics of configuration $N_4B_1W_4F_{11}$ in sideslip.

National Aeronautics and Space Administration
WASHINGTON, D. C.

OFFICIAL BUSINESS

FIRST CLASS MAIL

POSTAGE AND FEES PAID
NATIONAL AERONAUTICS AND
SPACE ADMINISTRATION

04U 001 56 51 3DS 00903
AIR FORCE WEAPONS LABORATORY/AFWL/
KIRTLAND AIR FORCE BASE, NEW MEXICO 8711

ATT MISS MADELINE F. CANOVA, CHIEF TECHN
LIBRARY /WLIL/

POSTMASTER: If Undeliverable (Section 158 Postal Manual) Do Not Return

"The aeronautical and space activities of the United States shall be conducted so as to contribute . . . to the expansion of human knowledge of phenomena in the atmosphere and space. The Administration shall provide for the widest practicable and appropriate dissemination of information concerning its activities and the results thereof."

—NATIONAL AERONAUTICS AND SPACE ACT OF 1958

NASA SCIENTIFIC AND TECHNICAL PUBLICATIONS

TECHNICAL REPORTS: Scientific and technical information considered important, complete, and a lasting contribution to existing knowledge.

TECHNICAL NOTES: Information less broad in scope but nevertheless of importance as a contribution to existing knowledge.

TECHNICAL MEMORANDUMS: Information receiving limited distribution because of preliminary data, security classification, or other reasons.

CONTRACTOR REPORTS: Scientific and technical information generated under a NASA contract or grant and considered an important contribution to existing knowledge.

TECHNICAL TRANSLATIONS: Information published in a foreign language considered to merit NASA distribution in English.

SPECIAL PUBLICATIONS: Information derived from or of value to NASA activities. Publications include conference proceedings, monographs, data compilations, handbooks, sourcebooks, and special bibliographies.

TECHNOLOGY UTILIZATION PUBLICATIONS: Information on technology used by NASA that may be of particular interest in commercial and other non-aerospace applications. Publications include Tech Briefs, Technology Utilization Reports and Notes, and Technology Surveys.

Details on the availability of these publications may be obtained from:

SCIENTIFIC AND TECHNICAL INFORMATION DIVISION

NATIONAL AERONAUTICS AND SPACE ADMINISTRATION

Washington, D.C. 20546